# Running coupling constant and mass anomalous dimension of six-flavor SU(2) gauge theory

M. Hayakawa,[1] K.-I. Ishikawa,[2] S. Takeda,[3] and N. Yamada[4,5,*]

[1]*Department of Physics, Nagoya University, Nagoya 464-8602, Japan*

[2]*Department of Physics, Hiroshima University, Higashi-Hiroshima 739-8526, Japan*

[3]*School of Mathematics and Physics, College of Science and Engineering, Kanazawa University, Kakuma-machi, Kanazawa, Ishikawa 920-1192, Japan*

[4]*KEK Theory Center, Institute of Particle and Nuclear Studies, High Energy Accelerator Research Organization (KEK), Tsukuba 305-0801, Japan*

[5]*School of High Energy Accelerator Science, The Graduate University for Advanced Studies (Sokendai), Tsukuba 305-0801, Japan*

(Received 14 August 2013; published 18 November 2013)

In the exploration of viable models of dynamical electroweak symmetry breaking, it is essential to locate the lower end of the conformal window and know the mass anomalous dimensions there for a variety of gauge theories. We calculate, with the Schrödinger functional scheme, the running coupling constant and the mass anomalous dimension of SU(2) gauge theory with six massless Dirac fermions in the fundamental representation. The calculations are performed on $6^4$–$24^4$ lattices over a wide range of lattice bare couplings to take the continuum limit. The discretization errors for both quantities are removed perturbatively. We find that the running slows down and comes to a stop at $0.06 \lesssim 1/g^2 \lesssim 0.15$ where the mass anomalous dimension is estimated to be $0.26 \lesssim \gamma_m^* \lesssim 0.74$.

DOI: 10.1103/PhysRevD.88.094504 PACS numbers: 12.38.Gc

## I. INTRODUCTION

A model of dynamical electroweak symmetry breaking, called technicolor (TC), offers a natural explanation to hierarchies present in the standard model (SM) [1–3]. This class of model could potentially suffer from several serious problems including those associated with the $S$ parameter [4], flavor changing neutral current [5], and relatively light Higgs mass [6]. All those problems are, however, expected to disappear if an underlying gauge theory follows "walking dynamics" [7]. By walking dynamics we mean that the renormalized gauge coupling runs in a strong coupling region only slowly over a wide range of the energy scale. Thus, a theory behaves as nearly scale invariant and as a strong coupled gauge theory. TC models possessing such a property are called walking technicolor (WTC). In order for a WTC scenario to work and avoid the problems above, another important feature is required, a large mass anomalous dimension $\gamma_m \sim \mathrm{O}(1)$ at the (nearly) conformal region; otherwise it fails, at least, to reproduce the observed masses of the standard model fermions. $\gamma_m$ is the $O(g^2)$ quantity in perturbation theory; thus $\gamma_m \sim \mathrm{O}(1)$ can be confirmed only by nonperturbative methods.

WTC consists of fermions having a vectorlike coupling to gauge fields and hence is tractable on the lattice. So far, a lot of effort has been made on the lattice to locate the lower end of the conformal window for various gauge systems, to gain a quantitative feature of walking dynamics and, importantly, to find the best candidate for WTC [8–39].[1] In our previous work, the scale dependence of the gauge coupling constant of ten-flavor QCD ($N_c = 3$ and $N_f = 10$) is investigated on the lattice, which provides an evidence of the infrared fixed point (IRFP) [37]. In this work, we focus on the two-color QCD with six massless Dirac fermions ($N_c = 2$ and $N_f = 6$) in the fundamental representation.

The lattice determination of the running coupling of this theory was performed by three groups [34–36], all of which adopt the Schrödinger functional (SF) scheme [43,44]. In Ref. [34] the calculations are carried out with the unimproved Wilson fermion. The continuum limit is attempted with a constant and linear fits using data obtained on $(L/a)^4 = 8^4$–$16^4$ lattices. With the constant fit, the renormalized coupling appears to reach a fixed point when $g^2 > 4.02$, although the data do not exclude the possibility of the absence of the fixed point in the range of couplings they studied because of large uncertainties. They also reported that the mass anomalous dimension at the possible fixed point is larger than 0.135 and that it can be as large as unity at the largest coupling ($g^2 = 5.52$) in their calculation.

In Ref. [35], the $O(a)$-improved Wilson-clover action is used on $(L/a)^4 = 6^4$–$16^4$ lattices for the running coupling and on $(L/a)^4 = 6^4$–$20^4$ for the running mass. After the continuum extrapolation linear in $a^2$, it is found that the running of the renormalized coupling begins to slow down at $g^2 \sim 5$ compared to the two-loop perturbation theory and the $\beta$ function eventually becomes consistent with zero at $g^2 \sim 12$, which is obviously larger than that of Ref. [34]. Under the assumption that the coupling reaches the IRFP, the mass anomalous dimension at the IRFP is estimated to be $\gamma^* \gtrsim 0.25$.

*norikazu.yamada@kek.jp

[1]For earlier works on many flavor QCD, see, for example, Refs. [40–42].

 

In Ref. [36], the status of their ongoing calculation of the running coupling using the stout-smeared Wilson fermion action is reported. One remarkable feature is that they succeed to explore the large renormalized coupling up to $g^2 \sim 35$. The continuum limit has not yet been taken, but from the behavior of the coupling data the authors infer the absence of IRFP, which is in contrast to the previous two works.

In this work, we use the Schrödinger functional scheme to calculate the running coupling and mass. The main differences from the previous works are the perturbative improvement of the discretization error and the inclusion of the larger lattice $24^4$. After our preliminary result was reported in Ref. [38], the statistics were substantially increased especially at our largest lattice ($24^4$). Based on the numerical results, we argue that the data is consistent with the presence of IRFP. The same argument is derived in our recent study on spectroscopy [39].

The paper is organized as follows. In Sec. II, we recall the results in perturbation theory. In Sec. III, the reason why walking theory with large anomalous dimension is necessary is reviewed. The Schrödinger functional scheme is briefly explained in Sec. IV. In Secs. V and VI, we describe the analysis method and present the numerical results of the running coupling and mass, respectively. In Sec. VII, we summarize our work and discuss the possible loophole in our argument and the future perspective. Some details and tables of numerical results are collected in the Appendices.

## II. PERTURBATION THEORY

In this section, we examine the perturbative predictions of the lower end of the conformal window, the value of the fixed point, and the mass anomalous dimension at the fixed point by adopting the $\overline{\text{MS}}$ scheme [45–47].

### A. Fixed point

We define the $\beta$ function by

$$\begin{aligned}\beta(g^2(L)) &= L\frac{\partial g^2(L)}{\partial L} \\ &= b_1 g^4(L) + b_2 g^6(L) + b_3 g^8(L) \\ &\quad + b_4 g^{10}(L) + \cdots, \end{aligned} \tag{1}$$

where $g(L)$ is the gauge coupling renormalized at length scale $L$. For SU($N_c$) gauge theory with $N_f$ flavors in the fundamental representation, the first four coefficients are known in the MS (and $\overline{\text{MS}}$) scheme [48] (see Appendix A). Provided that two coupling constants defined in two arbitrary schemes, $g_1$ and $g_2$, are related as

$$g_1^2 = g_2^2[1 + c_1 g_2^2 + O(g_2^4)], \tag{2}$$

the first two coefficients $b_1$ and $b_2$ are proven to be scheme independent. We can also see that, if $g_1$ is the single-valued function of $g_2$, the existence of the IRFP is scheme independent. For $N_c = 2$ and $N_f = 11$, $b_1$ vanishes and $b_2$ is negative. Thus, asymptotic freedom is lost for $N_f \geq 11$. The perturbative predictions for the IRFP, $g^2_{\text{FP}}$, in SU(2) gauge theory with $N_f$ flavors are summarized in Table I.

TABLE I. The perturbative predictions for the IRFP, $g^2_{\text{FP}}$, in the $\overline{\text{MS}}$ scheme for SU(2) gauge theory.

| $N_f$ | 5 | 6 | 7 | 8 | 9 | 10 |
|---|---|---|---|---|---|---|
| Two-loop | $\cdots$ | 143.56 | 35.59 | 15.79 | 7.48 | 2.90 |
| Three-loop $\overline{\text{MS}}$ | 38.10 | 20.68 | 13.25 | 8.65 | 5.26 | 2.47 |
| Four-loop $\overline{\text{MS}}$ | $\cdots$ | 30.10 | 15.21 | 9.55 | 5.58 | 2.52 |

TABLE II. The perturbative predictions for the IRFP, $g^2_{\text{FP}}$, in the $\overline{\text{MS}}$ scheme for SU(3) gauge theory.

| $N_f$ | 7 | 8 | 9 | 10 | 12 | 14 | 16 |
|---|---|---|---|---|---|---|---|
| Two-loop | $\cdots$ | $\cdots$ | 65.80 | 27.74 | 9.47 | 3.49 | 0.52 |
| Three-loop $\overline{\text{MS}}$ | 30.88 | 18.40 | 12.92 | 9.60 | 5.46 | 2.70 | 0.50 |
| Four-loop $\overline{\text{MS}}$ | $\cdots$ | 19.47 | 13.47 | 10.24 | 5.91 | 2.81 | 0.50 |

It should be noted that within the perturbation theory the existence of IRFP is mainly determined by the sign of the highest order term considered in the $\beta$ function. For example, at the two-loop (three-loop) approximation, $b_2 < 0$ for $N_f \geq 6$ ($N_f \geq 4$), and the IRFP exists in the same $N_f$ region. This is also true for SU(3) gauge theory as shown in Table II.

Since $b_3$ and higher order terms depend on the scheme, it is possible that the sign of $b_3$ depends on the scheme, which means that the smallest number of flavors having the IRFP, i.e., the lower end of the conformal window, depends on the scheme. Thus, at least, the analysis through the third order cannot give reliable information about the existence of the IRFP. With the fourth order term, one could discuss the convergence of the perturbative series. From the tables, it is seen, in general, that the difference of $g^2_{\text{FP}}$ from the three-loop and four-loop analyses is reasonably small ($\lesssim 15\%$) except for $N_f = 6$ in SU(2) gauge theory, where the IRFP increases by 50%.

However, even if $g^2_{\text{FP}}$ looks reasonably convergent, the IRFP is not observed in lattice studies of SU(3) gauge theory with eight flavors. This fact is interpreted in two ways: either the IRFP does not exist or the IRFP exists, but is too large to observe. Since the perturbative prediction of the IRFP in SU(2) gauge theory with six flavors is large and does not show plausible convergence, it would be difficult to draw a definite conclusion on the existence of the IRFP. Indeed, that is what is encountered in the previous works [34–36].

### B. Mass anomalous dimension

In the following discussion, it is implicitly assumed that we adopt one of the mass independent renormalization

schemes which respects chiral symmetry. We define the mass, flavor-singlet scalar density, and flavor nonsinglet pseudoscalar density operators renormalized at length scale $L$ by $\bar{m}(L)$, $S_R(L)$, and $P_R^a(L)$, respectively, as follows:

$$\bar{m}(L) = Z_m(L) m_0, \tag{3}$$

$$S_R(L) = Z_S(L) S_0, \tag{4}$$

$$P_R^a(L) = Z_P(L) P_0^a, \tag{5}$$

where the quantities with the subscript "0" denote the bare quantities. Then, the partially conserved axial-vector current relations lead to

$$Z_m(L) = \frac{1}{Z_P(L)} = \frac{1}{Z_S(L)}. \tag{6}$$

In the following, we extract the mass anomalous dimension $\gamma_m$ from the scale dependence of $Z_P(L)$.

We define the mass anomalous dimension by

$$\begin{aligned}\gamma_m(g^2(L)) &= \frac{L}{\bar{m}(L)}\frac{\partial \bar{m}(L)}{\partial L} = \frac{L}{Z_m(L)}\frac{\partial Z_m(L)}{\partial L} \\ &= -\frac{L}{Z_P(L)}\frac{\partial Z_P(L)}{\partial L} \\ &= d_1 g^2(L) + d_2 g^4(L) + d_3 g^6(L) \\ &\quad + d_4 g^8(L) + \cdots. \end{aligned} \tag{7}$$

The first four coefficients in the MS (and the $\overline{\text{MS}}$) scheme are available [49], and the explicit expressions are found in Appendix A. In this case, only $d_1$ is scheme independent. If an IRFP exists, the mass anomalous dimension at the fixed point is also scheme independent.

Now let us see the perturbative prediction. $\gamma_m^*$ turns out to drastically change by including higher order terms in $\beta$ and $\gamma_m$. For example, with the three-loop value of the fixed point ($g_{\text{FP}}^2 = 20.68$), the mass anomalous dimensions including one-, two-, three-, and four-loop corrections take 0.59, 1.19, 0.93, and $-0.26$, respectively. With the four-loop value of the fixed point ($g_{\text{FP}}^2 = 30.10$), they are 0.86, 2.14, 1.31, and $-4.02$. Thus, no stable prediction is obtained from perturbative analysis.

## III. PHENOMENOLOGICAL REQUIREMENT

In this section, we review that walking dynamics with a large anomalous dimension is needed in viable TC models. One crucial point in the WTC (or extended TC) scenario is how large quarks' and leptons' masses can be achieved [5], where the scalar condensate of the technifermions plays a key role. The fermion masses in the SM should be given by the RG invariant condensate

$$m_{\text{SM,f}} = \frac{C_S^{\text{X}}(1/\mu)}{M_{\text{ETC}}^2}\langle S_R^{\text{X}}(1/\mu)\rangle, \tag{8}$$

where $\mu$ is the renormalization scale, the superscript "X" labels the renormalization scheme chosen and $\langle\cdots\rangle$ denotes the vacuum expectation value. The coefficient $C_S^{\text{X}}(\mu)$ is the dimensionless coefficient and is of $O(1)$ at $\mu = M_{\text{ETC}}$. Its precise value depends on an explicit ETC model. Equation (8) does not depend on the scheme nor the scale.[2]

From Eq. (4), the condensate at $\mu = M_{\text{ETC}}$ can be written in terms of the condensate at any other scale as

$$\langle S_R^{\text{X}}(1/M_{\text{ETC}})\rangle = \frac{Z_S^{\text{X}}(1/M_{\text{ETC}})}{Z_S^{\text{X}}(a)}\langle S_R^{\text{X}}(a)\rangle, \tag{9}$$

where the lattice cutoff $a$ is chosen as an example. The first factor on the rhs describes the running of the scalar bilinear operator, or equivalently, the running of the renormalized mass, and is calculated in the following sections with the SF scheme. Thus X is set to SF. The second factor $\langle S_R^{\text{X}}(a)\rangle$ can be determined on the lattice in the lattice regularization scheme and thus needs a finite renormalization

$$S_R^{\text{SF}}(a) = C_S^{\text{SF-Lat}}(a) S_R^{\text{Lat}}(a), \tag{10}$$

connecting the SF and the lattice schemes, The factor $C_S^{\text{SF-Lat}}(a)$ can be calculated nonperturbatively as well on the lattice, although we do not calculate it in this paper.

After all, the masses of fermions in the SM is expressed as

$$m_{\text{SM,f}} = \frac{C_S^{\text{SF}}(1/M_{\text{ETC}})}{M_{\text{ETC}}^2}\frac{Z_S^{\text{SF}}(1/M_{\text{ETC}})}{Z_S^{\text{SF}}(a)} C_S^{\text{SF-Lat}}(a)\langle S_R^{\text{Lat}}(a)\rangle \tag{11}$$

$$= \frac{C_S^{\text{SF}}(1/M_{\text{ETC}})}{M_{\text{ETC}}^2}\frac{Z_S^{\text{SF}}(1/M_{\text{ETC}})}{Z_S^{\text{SF}}(a)} C_S^{\text{SF-Lat}}(a)\frac{\langle S_R^{\text{Lat}}(a)\rangle}{f_{\pi_{\text{T}}}^3} \times (246\ \text{GeV})^3, \tag{12}$$

where in the last equation the condensate is normalized by the technipion decay constant $f_{\pi_{\text{T}}} = 246$ GeV. The mass anomalous dimension is required in estimating the second factor $Z_S^{\text{SF}}(1/M_{\text{ETC}})/Z_S^{\text{SF}}(a)$ and is the main subject of this work.

In the classical TC model, the scalar condensate at $\mu = M_{\text{TC}}$ is estimated to be $M_{\text{TC}}^3$, and the other factors are naturally assumed to be of $O(1)$. Assuming $M_{\text{ETC}} \sim 1,000$ TeV and $M_{\text{TC}} \sim 1$ TeV, $m_{\text{SM,f}}$ ends up with $M_{\text{TC}}^3/M_{\text{ETC}} \sim 1$ MeV, and hence even the strange quark mass cannot be explained.

In the WTC model, it is expected that the huge enhancement of the second factor in Eq. (12) occurs due to walking with large $\gamma_m$. To explain this, we denote the second factor as

[2]In this argument, QCD and any other interactions and the corresponding scale dependences are ignored.

$$\sigma_P^{\mathrm{SF}}(u,s) = \frac{Z_P^{\mathrm{SF}}(L)}{Z_P^{\mathrm{SF}}(sL)} = \exp\left(\int_L^{sL} dL' \frac{\gamma_m^{\mathrm{SF}}(u(L'))}{L'}\right) = \exp\left(\int_u^{\sigma^{\mathrm{SF}}(u,s)} du' \frac{\gamma_m^{\mathrm{SF}}(u')}{\beta^{\mathrm{SF}}(u')}\right), \tag{13}$$

where $u = g^2(L)$ is introduced. The lower end of the integration range $\sigma^{\mathrm{SF}}(u,s)$ is the solution of

$$\int_u^{\sigma^{\mathrm{SF}}(u,s)} \frac{du'}{\beta^{\mathrm{SF}}(u')} = \ln(s). \tag{14}$$

When $u$ is very close to the fixed point, $\gamma_m$ becomes almost constant over a wide range of the renormalization scale. Then, $\sigma_P^{\mathrm{SF}}(u,s)$ can be approximated as

$$\sigma_P^{\mathrm{SF}}(u,s) \approx s^{\gamma_m^*}, \tag{15}$$

where $\gamma_m^*$ is the mass anomalous dimension at the fixed point. Substituting $s = M_{\mathrm{ETC}}/M_{\mathrm{TC}} \sim 1000$ and assuming $\gamma_m^* \sim 1$, $\sigma_P^{\mathrm{X}}(u,s)$ gives a huge enhancement by $s$ to the fermion masses in Eq. (12).

On the lattice, one can calculate $\sigma_P^{\mathrm{SF}}(u,s)$. If the IRFP exists, the mass anomalous dimension at the fixed point is extracted by

$$\gamma_m^* = \frac{\ln \sigma_P^{\mathrm{SF}}(u,s)}{\ln s}. \tag{16}$$

## IV. SIMULATION DETAILS

The scale dependence of the gauge coupling and the mass is calculated in the SF scheme [43,44]. The detailed setup is almost the same as our previous work [37] except for those subject to the number of colors, and is described in Appendix B. We adopt the unimproved Wilson fermion action and the Wilson plaquette gauge action, and no improvement is implemented at the action level. Instead, at the step of the analysis, the discretization errors are removed perturbatively as described below.

### A. Definition of the running coupling

With the gauge boundary conditions (B4) and (B5), the absolute minimum of the action is given by a color-electric background field denoted by $B(x)$. Then, the effective action can be defined as a function of $B$ by

$$\Gamma[B] = -\ln Z_{\mathrm{SF}}(C', \bar{\rho}', \rho'; C, \bar{\rho}, \rho), \tag{17}$$

which has the following perturbative expansion in the bare coupling constant:

$$\Gamma = \frac{1}{g_0^2}\Gamma_0 + \Gamma_1 + O(g_0^2), \tag{18}$$

and, in particular, the lowest-order term,

$$\Gamma_0 = [g_0^2 S_g[B]]_{g_0=0}, \tag{19}$$

is exactly the classical action of the induced background field. The SF scheme coupling is then defined in the massless limit of fermions by

$$\left.\frac{\partial\Gamma}{\partial\eta}\right|_{\eta=\pi/4,M=0} = \frac{1}{g_{\mathrm{SF}}^2(g_0^2,l)}\left.\frac{\partial\Gamma_0}{\partial\eta}\right|_{\eta=\pi/4,M=0} = \frac{k}{g_{\mathrm{SF}}^2(g_0^2,l)}\Bigg|_{M=0}, \tag{20}$$

where $l = L/a$ and $M$ is the mass in the lattice unit defined in the next subsection. $\eta = \pi/4$ is chosen following Ref. [50]. The normalization constant $k$ is determined such that $g_{\mathrm{SF}}^2 = g_0^2$ in the leading order of the perturbative expansion, and is found to be

$$k = \left.\frac{\partial\Gamma_0}{\partial\eta}\right|_{\eta=\pi/4,M=0} = -24l^2\sin\left[\frac{\pi}{2l^2}\right]. \tag{21}$$

Because of the absence of the $O(a)$ improvement for the fermion action, only the $\eta$ derivative of the gauge action contributes to $1/g_{\mathrm{SF}}^2(g_0^2,l)$.

### B. Definition of $Z_P$

In the SF setup, the renormalization constant of the pseudoscalar density and the fermion mass on the lattice are defined by

$$Z_P^{\mathrm{lat}}(g_0^2,L) = c\frac{\sqrt{3f_1}}{f_P(L/2)}\Bigg|_{M=0}, \tag{22}$$

$$M = \frac{1}{2}\frac{(\partial^* + \partial)f_A(x_0)}{2f_P(x_0)}\Bigg|_{x_0=L/2}, \tag{23}$$

respectively, where

$$f_P(x_0) = -\frac{1}{N_f^2-1}\sum_{\vec{y},\vec{z}}\langle\bar{\psi}(x)\gamma_5 T^a\psi(x)\bar{\zeta}(\vec{y})\gamma_5 T^a\zeta(\vec{z})\rangle, \tag{24}$$

$$f_A(x_0) = -\frac{1}{N_f^2-1}\sum_{\vec{y},\vec{z}}\langle\bar{\psi}(x)\gamma_\mu\gamma_5 T^a\psi(x)\bar{\zeta}(\vec{y})\gamma_5 T^a\zeta(\vec{z})\rangle, \tag{25}$$

$$f_1 = -\frac{1}{(N_f^2-1)L^6}\sum_{\vec{u},\vec{v},\vec{y},\vec{z}}\langle\bar{\zeta}'(\vec{u})\gamma_5 T^a\zeta'(\vec{v})\bar{\zeta}(\vec{y})\gamma_5 T^a\zeta(\vec{z})\rangle, \tag{26}$$

and $\zeta$ ($\zeta'$) is the boundary fermion at $x^0 = 0$ ($x^0 = L$) [43]. $\partial$ and $\partial^*$ are forward and backward lattice derivatives, respectively, and $T^a$ are the generators of the SU($N_f$) group. All quantities defined above are dimensionless. $c$ is determined such that $Z_P^{\mathrm{lat}}(g_0^2,L) = 1$ at tree level. We calculate $c$ in the background field method with our setup.

TABLE III. The numerical values of $\kappa_c$ at the tree level and $c$.

| $l = L/a$ | $m_c$ | $\kappa_c$ | $c = \frac{f_P(L/2)}{\sqrt{3}f_1}\|_{g_0^2=0,\kappa=\kappa_c}$ |
|---|---|---|---|
| 6 | −0.0375518783340131 | 0.126184617349584 | 1.2302955268807 |
| 8 | −0.0212857986789711 | 0.125668739874301 | 1.35598112469427 |
| 12 | −0.00949014679324021 | 0.125297272376912 | 1.47058643882059 |
| 16 | −0.00533796269846268 | 0.125167034239963 | 1.51920100305346 |
| 18 | −0.00421651481946245 | 0.125131905133095 | 1.53362308991718 |
| 24 | −0.00236949881524477 | 0.125074090727449 | 1.55933924368169 |

This results in a great advantage in the analysis of the small coupling region as explained later. The tree level values of the critical $\kappa$ and $c$ for various lattice sizes are tabulated in Table III.

### C. Parameters

The simulation was performed on the lattice sizes of $l^4 = (L/a)^4 = 6^4$, $8^4$, $12^4$, $16^4$, $18^4$, and $24^4$ in a wide range of $\beta = 4/g_0^2$ ($1.7 \le \beta \le 24.0$).

The algorithm to generate the gauge configurations follows the standard hybrid Monte Carlo with three pseudofermion fields and the Omelyan integrator with $\lambda = 0.0708$. The numerical simulations were carried out on several different architectures including a general purpose graphics processing unit and PC cluster. In order to achieve high performance on each architecture, the fermion solver part was optimized depending on architecture. In particular, the mixed precision solver and the flavor-parallelized blocked hybrid Monte Carlo algorithm using multiple graphics processing units enables us to obtain high statistics [51]. The acceptance rate is kept to around 80% by adjusting the molecular dynamics step size ($\delta\tau$). Since the Wilson fermion explicitly breaks chiral symmetry, the value of $\kappa$ is tuned for every pair of $(\beta, L/a)$ to its critical value $\kappa_c$ by monitoring the quark mass defined in Eq. (23).

## V. RUNNING COUPLING

### A. Numerical results

The SF coupling constant ($g^2_{\rm SF}$) and the dimensionless quark mass ($M$) obtained on each $(\beta, \kappa, l)$ are shown in Tables VIII–XIII in Appendix C together with other information such as the number of accumulated trajectories, the molecular dynamics step size $\delta\tau$, and the acceptance rate. The data with $|M|$ of typically $O(10^{-4})$ or, at most, 0.003 are only used in the following analysis.

$g_0^2/g^2_{\rm SF}$ is shown as a function of the bare coupling constant $g_0^2$ in Fig. 1. As a general behavior, at a given $g_0^2$, $g^2_{\rm SF}(g_0^2, l)$ increases with $l$, which is consistent with asymptotic freedom. For later use, the $g_0^2$ dependence of $g_0^2/g^2_{\rm SF}(g_0^2, l)$ is fitted, at each $l$, with the interpolating formula

$$\frac{g_0^2}{g^2_{\rm SF}(g_0^2, l)} = \frac{1 - a_{l,1} g_0^4}{1 + p_1(l) \times g_0^2 + \sum_{n=2}^{N} a_{l,n} \times g_0^{2n}}, \tag{27}$$

which is found to be the best among various functional forms we have tried. The degree of a polynomial $N$ is varied from 3 to 5 to look for the best fit. The coefficients $a_{l,n}$ thus determined are tabulated in Table IV, and the fit results are shown in Fig. 1 as the dotted curves.

In lattice perturbation theory, we calculated $p_1(l)$ in Eq. (27) and obtained

$$p_1(l) = \begin{cases} 0.26506184 & \text{for } L/a = 6 \\ 0.27347456 & \text{for } L/a = 8 \\ 0.28356222 & \text{for } L/a = 12 \\ 0.29062046 & \text{for } L/a = 16 \\ 0.29360965 & \text{for } L/a = 18 \\ 0.30127006 & \text{for } L/a = 24. \end{cases} \tag{28}$$

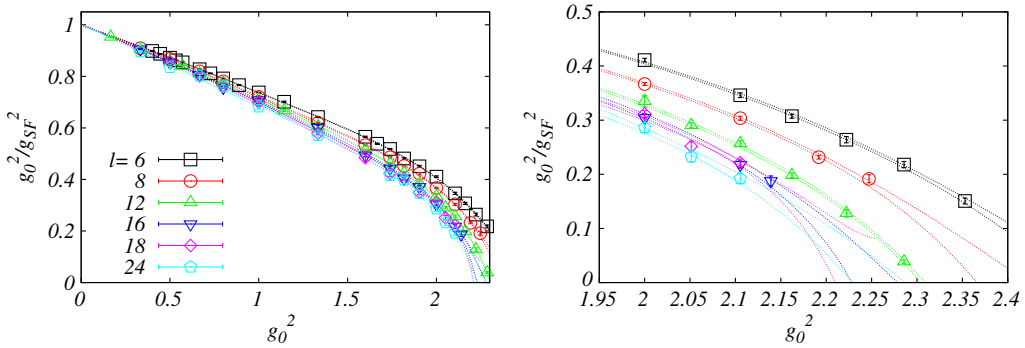


FIG. 1 (color online). $g_0^2$ dependence of $g_0^2/g^2_{\rm SF}$. The right panel magnifies the region of $g_0^2 \in [1.95, 2.40]$.

TABLE IV. The coefficients determined by fitting to Eq. (27). $N$ with * is the one chosen in the following analysis.

| $l$ | $N$ | $\chi^2$/d.o.f. | $a_{l,1}$ | $a_{l,2}$ | $a_{l,3}$ | $a_{l,4}$ | $a_{l,5}$ |
|---|---|---|---|---|---|---|---|
| 6 | 3 | 3.3 | 0.162(1) | −0.104(2) | −0.030(2) | | |
| 6 | 4 | 1.9 | 0.167(1) | −0.133(6) | 0.011(8) | −0.017(3) | |
| 6 | 5* | 0.9 | 0.162(2) | −0.175(13) | 0.142(37) | −0.121(29) | 0.026(7) |
| 8 | 3 | 2.6 | 0.172(2) | −0.089(6) | −0.042(5) | | |
| 8 | 4 | 1.3 | 0.180(2) | −0.137(14) | 0.024(18) | −0.026(7) | |
| 8 | 5* | 1.1 | 0.176(4) | −0.170(30) | 0.133(85) | −0.114(66) | 0.022(17) |
| 12 | 3 | 1.3 | 0.1873(4) | −0.089(4) | −0.055(3) | | |
| 12 | 4* | 0.4 | 0.1880(4) | −0.114(10) | −0.011(16) | −0.017(6) | |
| 12 | 5 | 0.5 | 0.1881(5) | −0.110(20) | −0.024(56) | −0.006(45) | −0.003(11) |
| 16 | 3 | 1.7 | 0.189(3) | −0.091(9) | −0.051(8) | | |
| 16 | 4* | 1.1 | 0.198(4) | −0.148(23) | 0.040(35) | −0.040(15) | |
| 16 | 5 | 1.2 | 0.196(7) | −0.168(47) | 0.110(141) | −0.100(116) | 0.017(31) |
| 18 | 3 | 1.6 | 0.184(6) | −0.073(17) | −0.051(17) | | |
| 18 | 4* | 0.9 | 0.201(6) | −0.190(46) | 0.112(62) | −0.067(23) | |
| 18 | 5 | 1.0 | 0.201(9) | −0.192(108) | 0.117(291) | −0.071(227) | 0.001(57) |
| 24 | 3* | 1.3 | 0.197(5) | −0.054(17) | −0.079(15) | | |
| 24 | 4 | 1.5 | 0.199(8) | −0.066(54) | −0.060(82) | −0.008(34) | |
| 24 | 5 | 1.5 | 0.207(7) | 0.012(94) | −0.316(247) | 0.211(195) | −0.059(50) |

These values will be used in the perturbative improvement of the discretization error.

### B. Discrete $\beta$ function

Hereafter the subscript "SF" is omitted as no confusion will arise. Since the raw data of $1/g^2(g_0^2, l)$ fluctuate around zero in the strong coupling region, converting to $g^2(g_0^2, l)$ sometimes induces a huge statistical uncertainty. To avoid this, we deal with the inverse coupling constant $1/g^2(g_0^2, l)$ in the analysis. The running of the coupling is analyzed with the discrete $\beta$ function (DBF) [15]

$$B(u, s) = \frac{1}{\sigma(u, s)} - \frac{1}{u}, \tag{29}$$

where

$$\sigma(u, s) = g^2(sL)|_{u=g^2(L)}. \tag{30}$$

$s > 1$ denotes the change of the renormalization scale. In this work, we take $s = 3/2$ or 2.

At the leading order (LO) of continuum perturbation theory, the DBF is constant,

$$B^{\mathrm{LO}}(u, s) = -b_1 \ln(s) = \begin{cases} -0.017117585 & \text{for } s = 3/2 \\ -0.029262705 & \text{for } s = 2. \end{cases} \tag{31}$$

The calculation including higher order terms is straightforward. Later, the nonperturbative results are compared with the two-loop perturbative result.

On the lattice, we define the lattice DBF in the same manner by

$$B^{\mathrm{lat}}(u, s, l) = \frac{1}{\Sigma(u, s, l)} - \frac{1}{u}, \tag{32}$$

$$\Sigma(u, s, l) = g^2(g_0^2, s \cdot l)|_{u=g^2(g_0^2, l)}. \tag{33}$$

The scale dependence of the coupling in the continuum limit is extracted by the step scaling technique as follows. Here, $g^2$ and $g_0^2$ denote the continuum and the lattice bare coupling, respectively. First, we choose an initial value of the renormalized coupling constant, denoted by $u$, which implicitly sets the initial length scale $L$ through $u = g^2(L)$. Using the interpolating formula, Eq. (27), at each lattice size $l$, the corresponding bare coupling constant ${g_0}^2$ is numerically determined by solving the equation $u = g^2({g_0}^2, l)$. The lattice step scaling function $\Sigma(u, s, l)$ is then defined as the SF coupling at the length scale $s \cdot l$ and the same bare coupling ${g_0}^2$, Eq. (33). Since both $l$ and $s \cdot l$ must be equal to one of 6, 8, 12, 16, 18, and 24, the possible values for the rescaling factor $s$ are limited. The difference between $\Sigma(u, s, l)$ and $u$ gives the scale dependence up to lattice artifacts.

By repeating the same procedure at a fixed $u$ but with different $l$ and taking the continuum limit, the lattice artifacts can be removed. We calculate the continuum limit of this function for various initial values $u$. In asymptotic-free theories, the DBF is negative at a small coupling region. If the sign of the continuum DBF flips at a certain renormalized coupling constant $u$, it indicates the existence of the IRFP around there.

### C. Improving discretization errors

Since we employ unimproved lattice actions, our results may be contaminated by substantial $O(a)$ discretization

errors. In principle, those errors can be removed by the continuum extrapolation, but it may require unreasonably large lattices as we will see below [52]. Thus, with limited resources, it is important to remove discretization errors as much as possible before taking the continuum limit. To do this, we perform the perturbative improvement on the step scaling function as follows.

In continuum perturbation theory, the step scaling function $\sigma(u, s)$ is given by

$$\sigma(u, s) = u + s_0 u^2 + s_1 u^3 + s_2 u^4 + \cdots, \tag{34}$$

$$s_0 = b_1 \ln(s), \tag{35}$$

$$s_1 = ({b_1}^2 \ln(s) + b_2) \ln(s), \tag{36}$$

$$s_2 = \left({b_1}^3 \ln^2(s) + \frac{5}{2} b_1 b_2 \ln(s) + b_3\right) \ln(s), \tag{37}$$

where $b_i$'s are the coefficients of the $\beta$ function introduced in Eq. (1). Let $B_0^{\rm lat}(u, s, l)$ and $\Sigma_0(u, s, l)$ be the unimproved lattice DBF and the step scaling function, respectively. Then the difference between the continuum and lattice DBF is

$$B(u, s) - B_0^{\rm lat}(u, s, l) = \frac{\Sigma_0(u, s, l) - \sigma(u, s)}{\sigma(u, s)\Sigma_0(u, s, l)} = \frac{\delta_0(u, s, l)}{\Sigma_0(u, s, l)}, \tag{38}$$

where we have introduced the measure of the discretization error as

$$\delta_0(u, s, l) = \frac{\Sigma_0(u, s, l) - \sigma(u, s)}{\sigma(u, s)} = \delta^{(1)}(s, l)u + O(u^2). \tag{39}$$

With $p_1(l)$ given in Eq. (28), the coefficient of the leading order term $\delta^{(1)}(s, l)$ is calculated as

$$\delta^{(1)}(s, l) = (p_1(sl) - b_1 \ln(sl)) - (p_1(l) - b_1 \ln(l)) = p_1(sl) - p_1(l) - b_1 \ln(s). \tag{40}$$

$\delta^{(1)}(s, l)$ is tabulated in Table V. It is seen that, for a fixed $s$, the change of $\delta^{(1)}(s, l)$ with $l$ is not monotonic. The same is observed in the improvement coefficient in ten-flavor QCD [37]. This nonmonotonic behavior indicates that when using unimproved actions without any improvement the continuum limit gives a wrong value unless $l$ is extremely large [52]. Thus, the one-loop improvement is important. The same may happen to the two-loop correction, which is not available. But, since the coefficients of the one-loop correction are reasonably small, we expect the effect is small at the two-loop level or higher.

TABLE V. Coefficients for perturbative correction, $\delta^{(1)}(s, l)$, for $(s, l)$.

| $(s, l)$ | $(3/2, 8)$ | $(3/2, 12)$ | $(3/2, 16)$ |
|---|---|---|---|
| $\delta^{(1)}(s, l)$ | −0.007030 | −0.007070 | −0.006468 |
| $(s, l)$ | $(2, 6)$ | $(2, 8)$ | $(2, 12)$ |
| $\delta^{(1)}(s, l)$ | −0.010762 | −0.012117 | −0.011555 |

Replacing $\Sigma_0(u, s, l)$ in Eqs. (38) and (39) with the one-loop improved one,

$$\Sigma_1(u, s, l) = \frac{\Sigma_0(u, s, l)}{1 + \delta^{(1)}(s, l)u}, \tag{41}$$

the discretization error reduces to $O(u^2)$. In the following, we mainly analyze the one-loop improved DBF defined by

$$B_1^{\rm lat}(u, s, l) = \frac{1}{\Sigma_1(u, s, l)} - \frac{1}{u}. \tag{42}$$

It should be noted that we have removed the $O(u)$ discretization error but not the whole $O(a)$ error. To be precise, the remaining discretization error of the lattice DBF, i.e., $B(u, s) - B_1^{\rm lat}(u, s, l)$, has a form of asymptotic expansion in $1/l$ [53] as

$$B_1^{\rm lat}(u, s, l) - B(u, s) = \left(\frac{1}{l} - \frac{1}{sl}\right) e(u) + O(l^{-2}), \tag{43}$$

where $e(u)$ is a coefficient associated with the leading discretization error and is an asymptotic series of $u$. After the one-loop improvement, $e(u)$ is of $O(u^2)$. Thus, the leading discretization error is still $O(a)$ with a reduced coefficient, and the extrapolation to the continuum limit will be performed linearly in $a$.

### D. Extraction of the continuum DBF

The continuum limit is taken for a fixed rescaling factor $s = 3/2$ or 2 and with an input value of $u$. The extrapolation is carried out for every jackknife ensemble, and the statistical error in the continuum limit is estimated by the single elimination jackknife method.

Figures 2 and 3 show the continuum limit of $B_1^{\rm lat}(u, s, l)$ for $s = 1.5$ and 2 at the four representative values of $1/u$ corresponding to $u = 2$–10, where the values in the continuum limit are shown in filled symbols. The results with (circles) and without (squares) perturbative improvement are shown there. It turns out that the improvement shifts the data and the continuum limit downward, and thus the continuum values with and without improvement disagree as expected from the nonmonotonic behavior of $\delta^{(1)}(s, l)$.

While at $1/u = 0.5$ the data show a small scaling violation or even no violation, the nonzero slope clearly appears in the strong coupling region. In general, the linear extrapolation appears to be valid, and hence the continuum limit is expected to be reliable. However, at $1/u = 0.1$ and $s = 2$, the data do not align, although the quality of the linear fit is still acceptable. A possible reason for this is that the step scaling function at the coarsest point for $s = 2$ contains the $l = 6$ data and the $O(a^2)$ discretization error becomes sizable at $1/u = 0.1$. To get rid of the possible

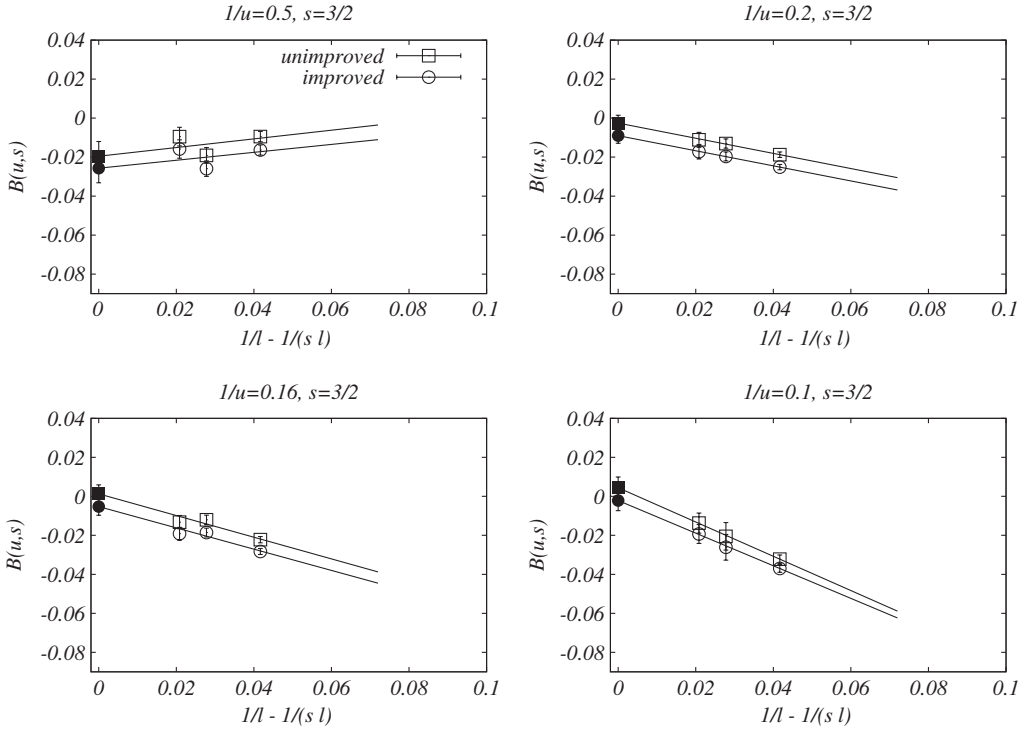


FIG. 2. Linear extrapolation of DBF to the continuum limit for $s = 1.5$.

contamination due to $O(a^2)$ errors, we fit the data without the coarsest point at $s = 2$; the results of which are shown in Fig. 3 as dotted lines and the filled triangles. It is seen that both fits agree well with each other except at $1/u = 0.1$. Importantly, the sign of the continuum DBF flips between $1/u = 0.16$ and 0.10, indicating the existence of the IRFP somewhere in this region. Since there is no reason to stick to using the full data, we adopt the

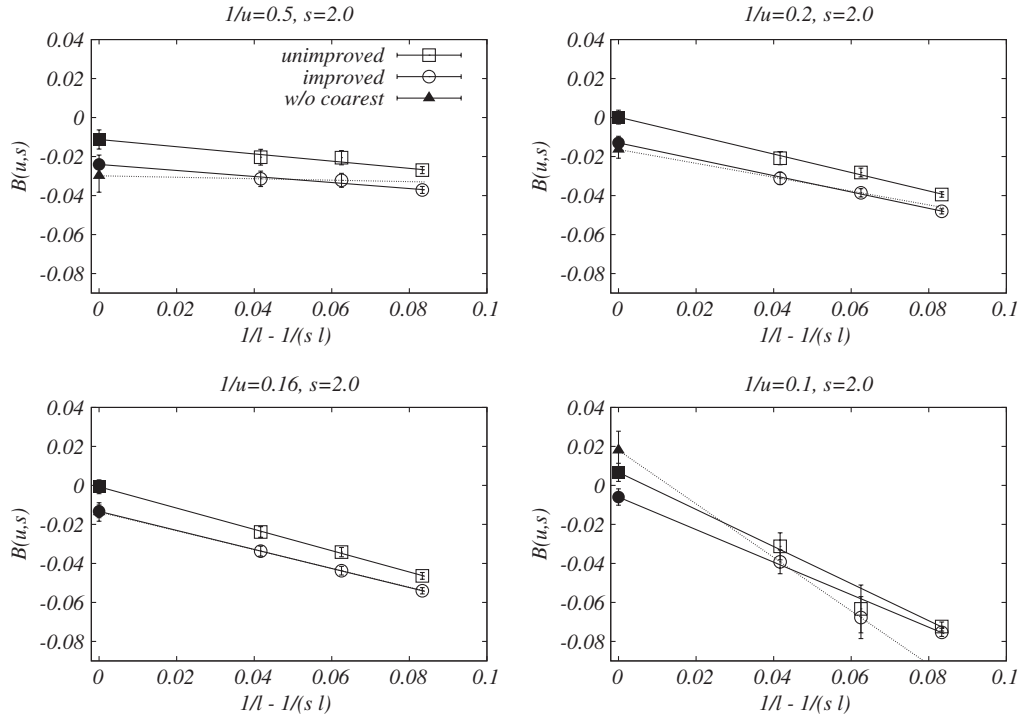


FIG. 3. Linear extrapolation of DBF to the continuum limit for $s = 2$.

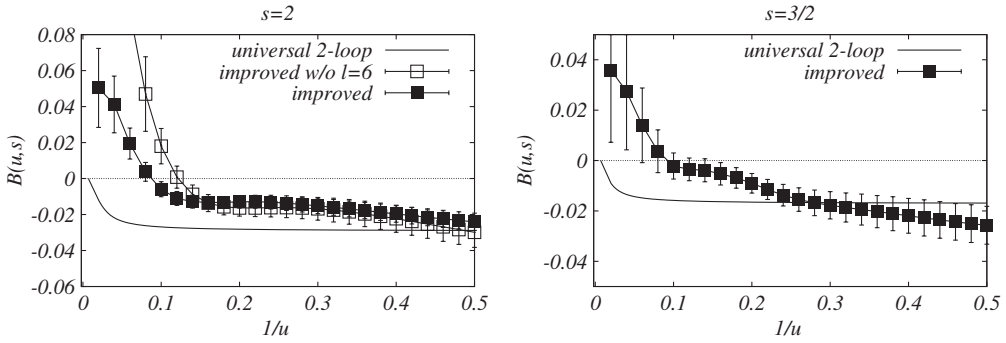


FIG. 4. $1/u$ dependence of $B(u, s)$ with $s = 2$ (left) and 1.5 (right). The universal two-loop perturbative prediction is also shown.

result of the latter analysis as our central value for $s = 2$, and the difference between two analyses is taken into account as the systematic uncertainty.

On the other hand, the data for $s = 3/2$ do not contain the $l = 6$ data, and indeed even at $1/u = 0.1$ the data well align. Thus, we do not omit the coarsest point for $s = 3/2$.

The DBF with one value of $s$ does not have to agree with that with a different value of $s$. However, if the IRFP exists, the DBF for arbitrary $s$ vanishes at the IRFP. Figure 4 shows the $1/u$ dependence of the continuum DBF with $s = 2$ (left) and $s = 3/2$ (right), where the results are compared with the perturbative result at the two-loop approximation.

The continuum DBF without the coarsest data point for $s = 2$ (open squares) is consistent with zero in $0.11 \leq 1/u \leq 0.13$, which means that in this region the running coupling constant reaches an IRFP. Note that, in the region of $u$ where the DBF is positive it is nontrivial for the continuum limit to exist. It is observed that the continuum limit using the full data set for $s = 2$ appears to reach IRFP at $1/u \sim 0.1$ smaller than the case without the coarsest data point.

The behavior of the continuum DBF with $s = 3/2$ (right panel of Fig. 4) is similar to that with $s = 2$. In this case, the possible location of the IRFP is slightly more ambiguous than the $s = 2$ case due to a larger statistical error. We observe that the continuum DBF is consistent with zero in $0.06 \leq 1/u \leq 0.15$ for $s = 3/2$. Since this uncertainty covers the possible range of the IRFP for $s = 2$ with and without the coarsest ($l = 6$) data point, we take the results at $s = 3/2$ as the conservative estimate for the IRFP.

## VI. RUNNING MASS

### A. Numerical results of $Z_P^{\rm lat}$

$Z_P^{\rm lat}(g_0^2, l)$ is calculated for various $g_0^2$ and $l$, and the data are fitted by

$$Z_P^{\rm lat}(g_0^2, l) = 1 + \sum_{i=1}^{N} z_i (g_0^2)^i, \tag{44}$$

for later use. Fit results are shown in Table VI and Fig. 5. The degree of the polynomial in Eq. (44) is chosen to be the minimal value yielding $\chi^2/\text{d.o.f.} \leq 2$.

Since the statistical errors of $Z_P^{\rm lat}$ are smaller than those of the coupling constant, the coefficients are well

TABLE VI. The coefficients determined in the fit of $Z_P^{\rm lat}(g_0^2, l)$. $N$ with * is the one chosen in the following analysis.

| $L/a$ | $N$ | $\chi^2$/d.o.f. | $z_{L/a,1}$ | $z_{L/a,2}$ | $z_{L/a,3}$ | $z_{L/a,4}$ | $z_{L/a,5}$ |
|---|---|---|---|---|---|---|---|
| 6 | 3 | 3.8 | −0.0974(10) | −0.0057(19) | −0.0293(7) | | |
| 6 | 4 | 3.5 | −0.0913(31) | −0.0234(87) | −0.0149(68) | −0.0035(16) | |
| 6 | 5* | 2.0 | −0.066(11) | −0.125(41) | 0.122(54) | −0.077(29) | 0.0136(52) |
| 8 | 3 | 4.8 | −0.1370(19) | 0.0110(32) | −0.0313(12) | | |
| 8 | 4 | 2.4 | −0.1197(47) | −0.045(14) | 0.016(12) | −0.0116(28) | |
| 8 | 5* | 1.9 | −0.1365(90) | 0.029(37) | −0.089(49) | 0.046(26) | −0.0109(48) |
| 12 | 3 | 7.4 | −0.1517(17) | 0.0051(41) | −0.0284(16) | | |
| 12 | 4* | 1.4 | −0.1410(23) | −0.0392(86) | 0.0166(82) | −0.0124(22) | |
| 16 | 3 | 3.8 | −0.1624(34) | 0.0065(67) | −0.0281(27) | | |
| 16 | 4* | 1.4 | −0.1398(64) | −0.069(19) | 0.043(17) | −0.0195(46) | |
| 18 | 3 | 2.0 | −0.1714(52) | 0.0147(93) | −0.0311(35) | | |
| 18 | 4* | 1.8 | −0.148(15) | −0.052(42) | 0.025(34) | −0.0141(84) | |
| 24 | 3 | 2.6 | −0.1743(51) | 0.007(10) | −0.0295(40) | | |
| 24 | 4* | 1.6 | −0.1529(92) | −0.070(29) | 0.044(27) | −0.0204(73) | |

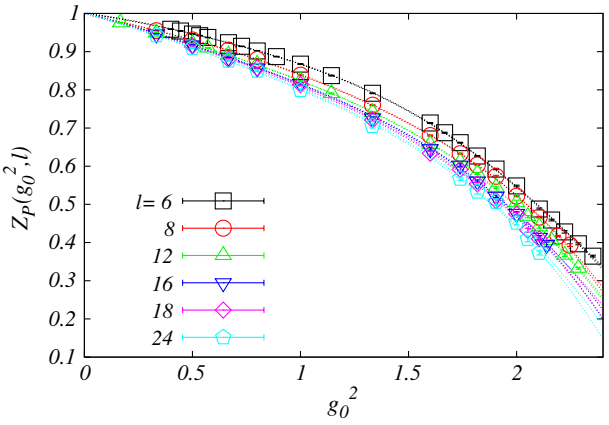


FIG. 5 (color online). $Z_P^{\rm lat}(g_0^2, l)$.

determined. One of the advantages in our calculation is that $Z_P^{\rm lat}$ defined in Eq. (22) includes a factor $c$, which we have explicitly calculated as shown in Table III. Because of this, the first term in the rhs of Eq. (44) can be set to unity, which makes the fit stable. If $c$ were not available, the first term would be replaced with another free parameter, making the statistical error somewhat larger. In Fig. 5, it is seen that $Z_P^{\rm lat}$ decreases with $l$ at a fixed $g_0^2$. It is the tendency which is necessary for WTC to work.

### B. Step scaling function and its improvement

The lattice step scaling function for $Z_P$ is defined by

$$\Sigma_{P,0}^{\rm lat}(u, s, l) = \left. \frac{Z_P^{\rm lat}(g_0^2, l)}{Z_P^{\rm lat}(g_0^2, s \cdot l)} \right|_{u=g_{\rm SF}^2(g_0^2,l)}. \tag{45}$$

We implement the one-loop improvement as for the running coupling. To this purpose, we define the measure of the discretization error by

$$\begin{aligned} \delta_{P,0}(u, s, l) &= \frac{\Sigma_{P,0}^{\rm lat}(u, s, l) - \sigma_P^{\rm PT}(u, s)}{\sigma_P^{\rm PT}(u, s)} \\ &= \delta_P^{(1)}(s, l)u + O(u^2), \end{aligned} \tag{46}$$

In principle, the improvement coefficient $\delta_P^{(1)}(s, l)$ can be calculated by perturbation theory. Since the coefficient respecting our SF setup is not available, we follow the prescription adopted in Ref. [54] and determine it by fitting $\delta_{P,0}$ to a linear function of $u$. In the fit to determine $\delta_P^{(1)}(s, l)$, $\sigma_P^{\rm PT}(u, s)$ in Eq. (46) has to be specified. We take the one-loop prediction

$$\sigma_P(u, s)|_{\rm LO} = \left(\frac{\sigma(u, s)}{u}\right)^{\frac{27}{40}}, \tag{47}$$

as $\sigma_P^{\rm PT}(u, s)$. The fit results are shown in Table VII. It is seen that the coefficient is small except for that with $l = 6$.

Once the improvement coefficient is determined, the improved step scaling function for $Z_P$ is obtained by

$$\Sigma_{P,1}^{\rm lat}(u, s, l) = \frac{\Sigma_{P,0}^{\rm lat}(u, s, l)}{1 + \delta_P^{(1)}(s, l)u}. \tag{48}$$

The continuum limit of $\Sigma_{P,i}^{\rm lat}$ ($i = 0$ or 1) is taken with a fixed $s(= 3/2\,\text{or}\,2)$ for the various initial value of the coupling constant $u$. In practice, the continuum limit is taken for $\ln \sigma_P(u, s)/\ln s$ introduced in Eq. (16) with a linear function in $a$. Figures 6 and 7 show the continuum limit of $\ln \sigma_P(u, s)/\ln s$ with and without the improvement at the four representative values of $1/u$ at $s = 3/2$ and 2, respectively.

Looking at these figures carefully, one question might arise. Namely, the unimproved data appears to have a scaling violation smaller than the improved one. In Fig. 8, we plot the $1/u$ dependence of the continuum limit without improvement for $s = 2$. As the figure clearly shows, in the small coupling region, where perturbation is reliable, the continuum limit is much smaller than the perturbative prediction. From this observation, we infer that the small scaling violation for the unimproved data is fake and that the improvement removes such nonlinear discretization errors efficiently and makes the data align. In the following, we only analyze the improved data.

In Fig. 6, the three improved data points at $s = 3/2$ well align independently of the value of $1/u$, while it is hard to justify the linear extrapolation using three data for $s = 2$ as seen in Fig. 7. Thus, at $s = 2$ we omit the coarsest data point and take the continuum limit as before. The fit results without the coarsest point are shown in Fig. 7.

$\ln \sigma_P(u, s)/\ln s$ depends on $s$, but if the IRFP exists its value becomes $\gamma_m^*$ independently of $s$ at the IRFP. To check this, we plot $\ln \sigma_P(u, s)/\ln s$ for $s = 3/2$ and 2 as a function of $1/u$ in Fig. 9. The perturbative prediction shown in the figure is calculated using the combination of the two-loop $\beta$ function and the one-loop anomalous dimension for $s = 2$, and that for $s = 3/2$ is omitted because the difference is too tiny to distinguish.

Recalling the range of the possible IRFP value $0.06 \leq 1/u \leq 0.15$, it is seen that two results agree with each other in that range, which is interpreted as another support to the existence of the IRFP and justify our analysis. Provided that the value of IRFP is in $0.06 \lesssim 1/u \lesssim 0.15$, it is found that $0.26 \lesssim \gamma_m^* \lesssim 0.74$.

TABLE VII. Coefficients for perturbative correction, $\delta_P^{(1)}(s, l)$ for each pair of $(s, l)$. The square brackets in the first column indicate the fit range in $u$.

| $(s, l)$ | (3/2, 8) | (3/2, 12) | (3/2, 16) |
|---|---|---|---|
| $\delta_P^{(1)}(s, l)$ | 0.0051(7) | −0.0001(13) | 0.0001(14) |
| $(s, l)$ | (2, 6) | (2, 8) | (2, 12) |
| $\delta_P^{(1)}(s, l)$ | 0.0216(5) | 0.0040(9) | −0.0002(13) |

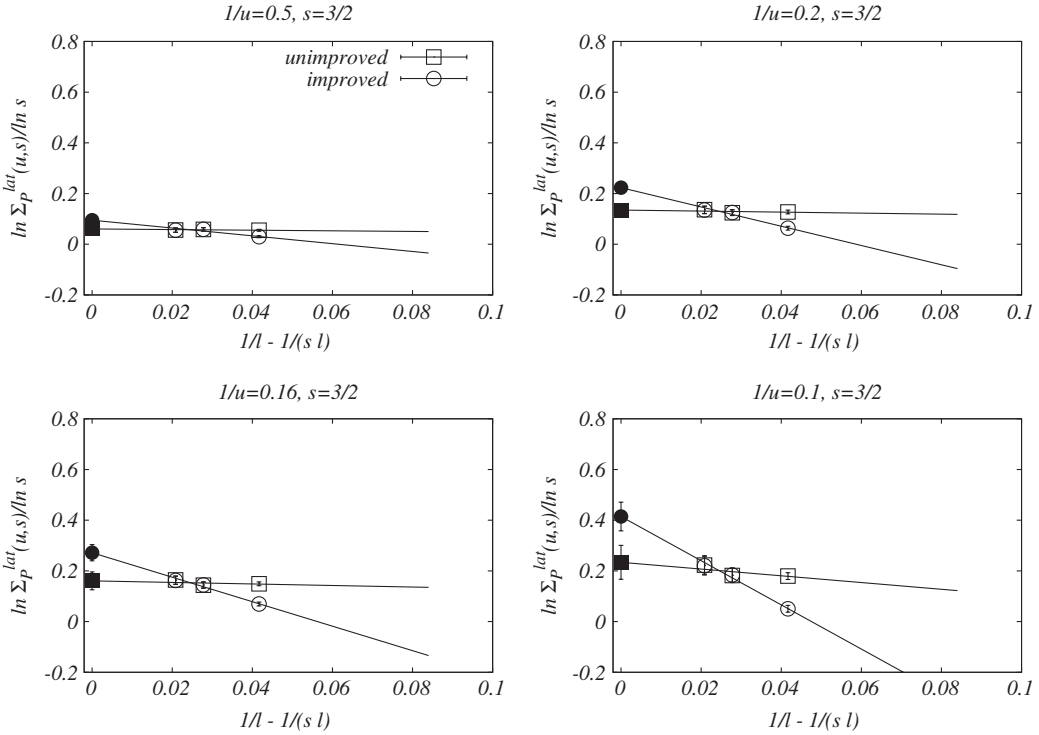


FIG. 6. Continuum limit of $\ln \sigma_P(u, s)/\ln s$ for $s = 1.5$.

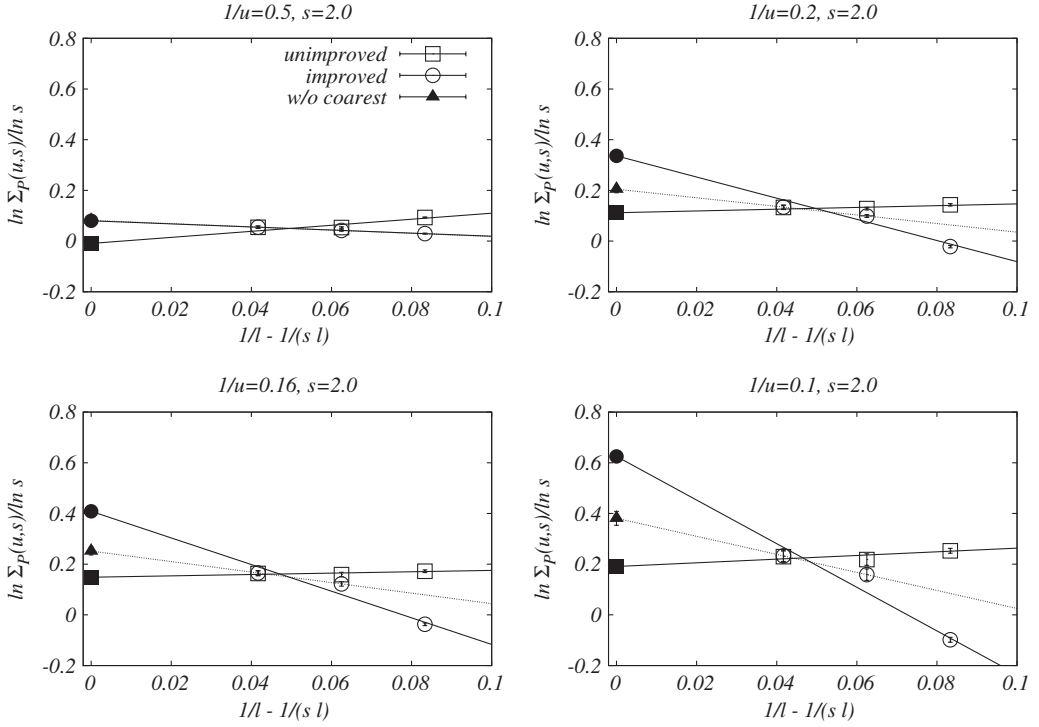


FIG. 7. Continuum limit of $\ln \sigma_P(u, s)/\ln s$ for $s = 2$.

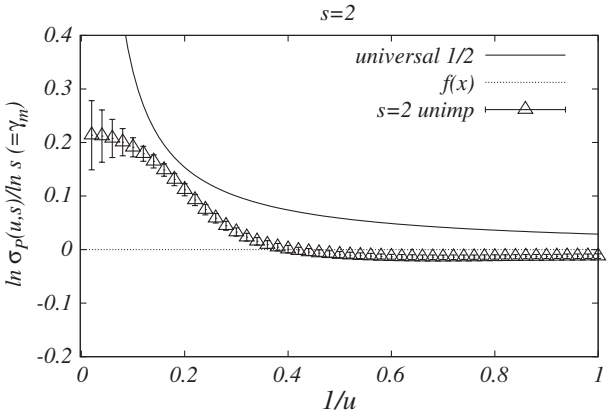


FIG. 8. Continuum limit of $\gamma_m$ at $s = 2$ without improvement.

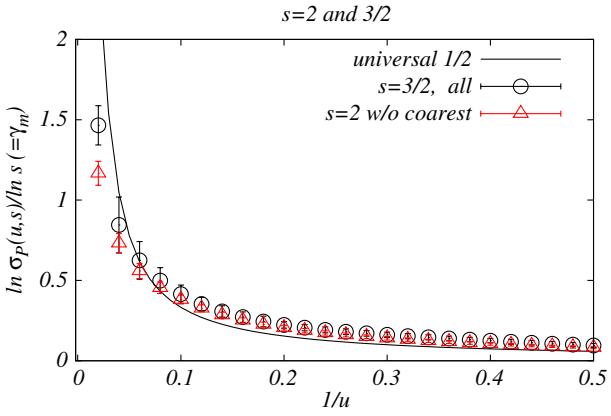


FIG. 9 (color online). Continuum limit of $\gamma_m$.

## VII. SUMMARY AND DISCUSSION

In this work, the running coupling constant and the mass anomalous dimension of six-flavor two-color QCD are numerically investigated using the lattice step scaling technique. The discretization errors are improved perturbatively and the improvement turns out to decrease the DBF, which explains the discrepancy between Ref. [34,35] qualitatively. The extrapolation of the DBF to the continuum limit is taken linearly assuming that the $O(a)$ scaling violation dominates the higher order ones. The DBF in the continuum limit turns out to approach zero from below as the inverse SF coupling constant $1/u$ decreases, and it becomes consistent with zero in the range $0.06 \leq 1/u \leq 0.15$. The linear extrapolation is reasonably justified within the statistical error, but a further rigorous check is clearly preferable. The result of this work suggests that SU(2) gauge theory with six Dirac fermions in the fundamental representation is in the conformal window.

One possible loophole in our analysis may be related to the validity of the linear extrapolation. Since the number of data points used in the continuum extrapolation is rather limited, we cannot check the validity rigorously. Within this limitation, we have made a nontrivial check that the continuum limits of the DBF or $\ln \sigma_P / \ln s$ with two different values of $s$ agree. Such a check sustains the possibility that the systematic uncertainty due to neglecting $O(a^2)$ or higher order scaling violations is not significantly large.

In order to confirm the existence of the IRFP or even determine the more precise value of the fixed point, data from larger lattices with high statistics are necessary. It is, however, difficult to do with machines currently available to us, and probably more efficient methods or approaches are necessary to go further. The conformal window can also be studied by looking at hadron spectroscopy or renormalization group analysis on the lattice. In order to establish the location of the lower end of the conformal window, the consistency check employing these methods would be indispensable. What is the most important in the context of the WTC is the value of the anomalous dimension of the $\overline{\psi}\psi$ operator, and it is found that $0.26 \lesssim \gamma_m^* \lesssim 0.74$ in the possible range of the IRFP.

The anomalous dimension of the six-flavor theory turns out to be smaller than the value required in phenomenology, and hence the five- or four-flavor theory may be interesting to study. Provided that one eventually succeeds to find an attractive candidate for WTC through conformal window search, the next step would be the calculation of the $S$ parameter. The calculational method has been established in Ref. [55], where the QCD $S$ parameter is calculated on the lattice for the first time and is correctly reproduced. In Ref. [10], the evidence of the reduction of $S$ parameter is observed in the presence of many flavors. Another important direction is obviously to calculate the mass spectrum of the candidate theories, including vector and scalar resonances, the decay constant of the Nambu Goldstone boson, and the chiral condensate. Our first result is reported in Ref. [39]. Although the precise determinations of these quantities are challenging, the direct comparison with the upcoming LHC results is extremely interesting, and we believe that such calculations are worth a lot of effort.

## ACKNOWLEDGMENTS

N. Y. would like to thank Hideo Matsufuru for useful discussions as well as providing us with a comfortable machine environment. The main part of the numerical simulations were performed on the B-factory computer system at KEK and on the computer system $\varphi$ at Nagoya University. This work is supported in part by the Grant-in-Aid for Scientific Research of the Japanese Ministry of Education, Culture, Sports, Science, and Technology and JSPS (No. 20540261, No. 22224003, No. 22740183, and No. 23740177).

## APPENDIX A: PERTURBATIVE COEFFICIENTS

### 1. $\beta$ function

In the MS (and $\overline{\text{MS}}$ scheme), the coefficients of the $\beta$ function for SU($N_c$) gauge theory with $N_f$ flavors in the fundamental representation are known to the four-loop level [48] as

$$b_1 = \frac{2}{(4\pi)^2}\left[\frac{11C_A}{3} - \frac{4T_F}{3}N_f\right], \tag{A1}$$

$$b_2 = \frac{2}{(4\pi)^4}\left[\frac{34C_A^2}{3} - \left(\frac{20C_A}{3} + 4C_F\right)T_F N_f\right], \tag{A2}$$

$$b_3^{\overline{\rm MS}} = \frac{2}{(4\pi)^6}\left[\frac{2857}{54}C_A^3 + \left(2C_F^2 - \frac{205}{9}C_F C_A - \frac{1415}{27}C_A^2\right)T_F N_f + \left(\frac{44}{9}C_F + \frac{158}{27}C_A\right)T_F^2 N_f^2\right], \tag{A3}$$

$$\begin{aligned} b_4^{\overline{\rm MS}} = \frac{2}{(4\pi)^8}\Bigg[ & C_A^4\left(\frac{150653}{486} - \frac{44}{9}\zeta_3\right) + C_A^3 T_F N_f\left(-\frac{39143}{81} + \frac{136}{3}\zeta_3\right) + C_A^2 C_F T_F N_f\left(\frac{7073}{243} - \frac{656}{9}\zeta_3\right) \\ & + C_A C_F^2 T_F N_f\left(-\frac{4204}{27} + \frac{352}{9}\zeta_3\right) + 46 C_F^3 T_F N_f + C_A^2 T_F^2 N_f^2\left(\frac{7930}{81} + \frac{224}{9}\zeta_3\right) + C_F^2 T_F^2 N_f^2\left(\frac{1352}{27} - \frac{704}{9}\zeta_3\right) \\ & + C_A C_F T_F^2 N_f^2\left(\frac{17152}{243} + \frac{448}{9}\zeta_3\right) + \frac{424}{243}C_A T_F^3 N_f^3 + \frac{1232}{243}C_F T_F^3 N_f^3 + N_c^2\frac{N_c^2+36}{24}\left(-\frac{80}{9} + \frac{704}{3}\zeta_3\right) \\ & + N_f N_c\frac{N_c^2+6}{48}\left(\frac{512}{9} - \frac{1664}{3}\zeta_3\right) + N_f^2\frac{N_c^4 - 6N_c^2 + 18}{96N_c^2}\left(-\frac{704}{9} + \frac{512}{3}\zeta_3\right)\Bigg], \end{aligned} \tag{A4}$$

where

$$\zeta_3 = 1.202056903, \qquad \zeta_4 = 1.0823232, \qquad \zeta_5 = 1.0369277, \tag{A5}$$

and $T_F = \frac{1}{2}$. For $N_c = 2$,

$$C_A = N_c = 2, \qquad C_F = \frac{N_c^2 - 1}{2N_c} = \frac{3}{4}. \tag{A6}$$

### 2. Anomalous dimension

In the MS (and $\overline{\rm MS}$ scheme), the coefficients of the mass anomalous dimension for SU($N_c$) gauge theory with $N_f$ flavors in the fundamental representation are known to the four-loop level [49] as

$$d_1 = \frac{2}{(4\pi)^2}3C_F, \tag{A7}$$

$$d_2 = \frac{2}{(4\pi)^4}\left[\frac{3}{2}C_F^2 + \frac{97}{6}C_F C_A - \frac{10}{3}C_F T_F N_f\right], \tag{A8}$$

$$\begin{aligned} d_3 = \frac{2}{(4\pi)^6}\Bigg[ & \frac{129}{2}C_F^3 - \frac{129}{4}C_F^2 C_A + \frac{11413}{108}C_F C_A^2 + C_F^2 T_F N_f(-46 + 48\zeta_3) \\ & + C_F C_A T_F N_f\left(-\frac{556}{27} - 48\zeta_3\right) - \frac{140}{27}C_F T_F^2 N_f^2\Bigg], \end{aligned} \tag{A9}$$

$$\begin{aligned} d_4 = \frac{2}{(4\pi)^8}\Bigg[ & C_F^4\left(-\frac{1261}{8} - 336\zeta_3\right) + C_F^3 C_A\left(\frac{15349}{12} + 316\zeta_3\right) + C_F^2 C_A^2\left(-\frac{34045}{36} - 152\zeta_3 + 440\zeta_5\right) \\ & + C_F C_A^3\left(\frac{70055}{72} + \frac{1418}{9}\zeta_3 - 440\zeta_5\right) + C_F^3 T_F N_f\left(-\frac{280}{3} + 552\zeta_3 - 480\zeta_5\right) \\ & + C_F^2 C_A T_F N_f\left(-\frac{8819}{27} + 368\zeta_3 - 264\zeta_4 + 80\zeta_5\right) + C_F C_A^2 T_F N_f\left(-\frac{65459}{62} - \frac{2684}{3}\zeta_3 + 264\zeta_4 + 400\zeta_5\right) \\ & + C_F^2 T_F^2 N_f^2\left(\frac{304}{27} - 160\zeta_3 + 96\zeta_4\right) + C_F C_A T_F^2 N_f^2\left(\frac{1342}{81} + 160\zeta_3 - 96\zeta_4\right) + C_F T_F^3 N_f^3\left(-\frac{664}{81} + \frac{128}{9}\zeta_3\right) \\ & + \frac{(N_c^2-1)(N_c^2+6)}{48}(-32 + 240\zeta_3) + N_f\frac{(N_c^2-1)(N_c^4 - 6N_c^2 + 18)}{96N_c^3}(64 - 480\zeta_3)\Bigg]. \end{aligned} \tag{A10}$$

## APPENDIX B: SCHRÖDINGER FUNCTIONAL SCHEME

The SF on the lattice is defined on a four-dimensional hypercubic lattice with a volume $(L/a)^4$ in the cylindrical geometry, and the physical length $L$ is identified as the renormalization scale. The periodic boundary condition in the spatial directions with a vanishing phase factor ($\theta = 0$) and the Dirichlet one in the temporal direction are imposed for both gauge $[U_\mu(x)]$ and fermion $[\psi(x)$ and $\bar{\psi}(x)]$ fields. The boundary values for gauge and fermion fields are represented by two-by-two color matrices, $C$ and $C'$, and spinors, $\rho$, $\rho'$, $\bar{\rho}$, and $\bar{\rho}'$, respectively. The partition function of this system is given by

$$Z_{\mathrm{SF}}(C', \bar{\rho}', \rho'; C, \bar{\rho}, \rho) = e^{-\Gamma(C', \bar{\rho}', \rho'; C, \bar{\rho}, \rho)} = \int D[U, \psi, \bar{\psi}] e^{-S[U, \psi, \bar{\psi}, C, C', \rho, \rho', \bar{\rho}, \bar{\rho}']}, \tag{B1}$$

where $\Gamma$ is the effective action, and

$$S[U, \psi, \bar{\psi}, C, C', \rho, \rho', \bar{\rho}, \bar{\rho}'] = S_g[U, C, C'] + S_q[U, \psi, \bar{\psi}, \rho, \rho', \bar{\rho}, \bar{\rho}']. \tag{B2}$$

We take the plaquette gauge action,

$$S_g[U, C, C'] = \frac{\beta}{4} \sum_x \sum_{\mu=0}^{3} \sum_{\nu=0}^{3} \bar{\delta}_{\mu,\nu} w_{\mu,\nu}(x_0) \,\mathrm{Tr}[1 - P_{\mu,\nu}(x)], \tag{B3}$$

where $\beta = 4/g_0^2$ set the lattice bare coupling constant $g_0^2$, $\bar{\delta}_{\mu,\nu} = 0$ when $\mu = \nu$ otherwise 1, and $P_{\mu,\nu}(x)$ denotes a $1 \times 1$ Wilson loop on the $\mu$-$\nu$ plane starting and ending at $x$. The spatial link variables at $x_0 = 0$ and $L/a$ are all set to the diagonal, constant matrices [50],

$$U_k(x)|_{x_0=0} = \exp[C], \qquad C = \frac{a}{iL} \begin{pmatrix} \eta & 0 \\ 0 & -\eta \end{pmatrix}, \tag{B4}$$

$$U_k(x)|_{x_0=L/a} = \exp[C'], \qquad C' = \frac{a}{iL} \begin{pmatrix} \pi - \eta & 0 \\ 0 & -\pi + \eta \end{pmatrix}, \tag{B5}$$

where $k = 1, 2, 3$, and $\eta$ is parametrizing the gauge boundary fields and is eventually set to $\pi/4$. The weight $w_{\mu,\nu}(x_0)$ in Eq. (B3) is given by

$$w_{\mu,\nu}(x_0) = \begin{cases} c_{x_0} & \text{for } (x_0 = 0 \quad \text{or} \quad x_0 = L/a - 1) \quad \text{and} \quad (\mu \quad \text{or} \quad \nu = 0) \\ 0 & \text{for } (x_0 = L/a) \quad \text{and} \quad (\mu \quad \text{or} \quad \nu = 0) \\ \frac{1}{2} c_s & \text{for } (x_0 = 0 \quad \text{or} \quad x_0 = L/a) \quad \text{and} \quad (\mu \neq 0 \quad \text{and} \quad \nu \neq 0) \\ 1 & \text{for all the other cases.} \end{cases} \tag{B6}$$

By tuning $c_t$, $O(a)$ errors induced by the boundaries in the time direction can be removed perturbatively, but in this work we simply take its tree level values, $c_t = 1$. With this setup, the value of $c_s$ is arbitrary because the spatial plaquettes on the boundaries do not contribute to the action. We thus set $c_s = 0$.

The fermion fields are described by the unimproved Wilson fermion action,

$$S_q[U, \psi, \bar{\psi}] = N_f \sum_{x,y} \bar{\psi}(x) D(x, y; U) \psi(y) = N_f \sum_{x,y} \bar{\psi}^{\mathrm{lat}}(x) D^{\mathrm{lat}}(x, y; U) \psi^{\mathrm{lat}}(y), \tag{B7}$$

$$D^{\mathrm{lat}}(x, y; U) = \delta_{xy} - \kappa \sum_{\mu} \{(1 - \gamma_\mu) U_\mu(x) \delta_{x+\hat{\mu},y} + (1 + \gamma_\mu) U_\mu^\dagger(x - \hat{\mu}) \delta_{x-\hat{\mu},y}\}, \tag{B8}$$

where

$$\psi^{\mathrm{lat}}(x) = \frac{1}{\sqrt{2\kappa}} \psi(x), \qquad \bar{\psi}^{\mathrm{lat}}(x) = \frac{1}{\sqrt{2\kappa}} \bar{\psi}(x), \qquad D^{\mathrm{lat}}(x, y; U) = 2\kappa D(x, y; U). \tag{B9}$$

The hopping parameter $\kappa$ is related to the dimensionless bare mass $M_0$ through $2\kappa = 1/(M_0 + 4)$. The dynamical degrees of freedom of the fermion field $\psi(x)$ and antifermion fields $\bar{\psi}(x)$ reside on the lattice sites $x$ with $0 < x_0 < T$. On both boundaries ($x_0 = 0$ and $L/a$), half of the Dirac components are set to zero and the remaining components are fixed to some prescribed values, $\rho$, $\bar{\rho}$, $\rho'$, and $\bar{\rho}'$, as

$$P_+\psi(x)|_{x_0=0} = \rho(\mathbf{x}), \qquad P_-\psi(x)|_{x_0=0} = 0, \tag{B10}$$

$$P_-\psi(x)|_{x_0=L/a} = \rho'(\mathbf{x}), \qquad P_+\psi(x)|_{x_0=L/a} = 0, \tag{B11}$$

$$\bar{\psi}(x)P_-|_{x_0=0} = \bar{\rho}(\mathbf{x}), \qquad \bar{\psi}(x)P_+|_{x_0=0} = 0, \tag{B12}$$

$$\bar{\psi}(x)P_+|_{x_0=L/a} = \bar{\rho}'(\mathbf{x}), \qquad \bar{\psi}(x)P_-|_{x_0=L/a} = 0, \tag{B13}$$

where $P_\pm = (1 \pm \gamma_0)/2$. In this work, the boundary values for the fermion fields are set to zero, i.e.,

$$\rho = \rho' = \bar{\rho} = \bar{\rho}' = 0. \tag{B14}$$

## APPENDIX C: RAW DATA

TABLE VIII. Simulation parameters and results at $L/a = 6$.

| $\beta$ | $\kappa$ | Trajectories | Plaquette | $\delta\tau$ | Acceptance | $g^2_{\mathrm{SF}}$ | $M$ |
|---|---|---|---|---|---|---|---|
| 10.00 | 0.1295040 | 30,000 | 0.926136(16) | 0.1429 | 0.789(2) | 0.44518(41) | 0.00007(4) |
| 9.00 | 0.1299100 | 30,000 | 0.917889(12) | 0.1429 | 0.824(2) | 0.50087(63) | −0.00005(4) |
| 8.00 | 0.1304270 | 30,000 | 0.907552(12) | 0.1667 | 0.748(3) | 0.57331(81) | 0.00007(9) |
| 7.50 | 0.1307300 | 30,000 | 0.901344(14) | 0.1667 | 0.773(2) | 0.61855(86) | 0.00045(10) |
| 7.00 | 0.1311050 | 30,000 | 0.894285(18) | 0.1667 | 0.788(3) | 0.66875(70) | 0.00002(6) |
| 6.00 | 0.1320476 | 30,000 | 0.876503(19) | 0.1667 | 0.815(2) | 0.8055(11) | 0.00015(7) |
| 5.50 | 0.1326700 | 30,000 | 0.865107(37) | 0.1667 | 0.824(3) | 0.8962(17) | 0.00012(10) |
| 5.00 | 0.1334600 | 30,000 | 0.851424(25) | 0.1667 | 0.840(3) | 1.0101(20) | −0.00012(13) |
| 4.50 | 0.1344250 | 45,000 | 0.834738(23) | 0.2000 | 0.750(2) | 1.1605(26) | 0.00013(13) |
| 4.00 | 0.1357000 | 30,000 | 0.813595(32) | 0.2000 | 0.774(3) | 1.3564(24) | 0.00048(21) |
| 3.50 | 0.1375000 | 30,000 | 0.786531(51) | 0.2000 | 0.794(2) | 1.6297(69) | −0.00060(23) |
| 3.00 | 0.1400480 | 60,000 | 0.750086(30) | 0.2000 | 0.814(2) | 2.0760(76) | 0.00078(15) |
| 2.50 | 0.1441900 | 60,000 | 0.699079(34) | 0.2000 | 0.820(2) | 2.829(12) | −0.00022(24) |
| 2.40 | 0.1453500 | 60,000 | 0.686330(35) | 0.2000 | 0.820(2) | 3.095(13) | −0.00050(26) |
| 2.30 | 0.1466400 | 60,000 | 0.672451(28) | 0.2000 | 0.824(1) | 3.356(15) | −0.00045(25) |
| 2.20 | 0.1481000 | 60,000 | 0.657554(42) | 0.2000 | 0.822(2) | 3.776(24) | 0.00033(30) |
| 2.10 | 0.1498190 | 60,500 | 0.641272(58) | 0.2000 | 0.825(2) | 4.222(31) | −0.00029(38) |
| 2.00 | 0.1517700 | 60,000 | 0.623513(50) | 0.2000 | 0.823(2) | 4.867(39) | 0.00030(63) |
| 1.90 | 0.1541500 | 60,000 | 0.604247(65) | 0.2000 | 0.822(1) | 6.084(78) | 0.00041(83) |
| 1.85 | 0.1554600 | 105,000 | 0.594149(43) | 0.2000 | 0.822(1) | 7.036(87) | −0.00013(67) |
| 1.80 | 0.1568700 | 74,500 | 0.583519(62) | 0.2000 | 0.824(2) | 8.42(18) | −0.00019(94) |
| 1.75 | 0.1584100 | 60,000 | 0.572455(94) | 0.2000 | 0.824(2) | 10.49(28) | −0.0007(11) |
| 1.70 | 0.1599900 | 60,000 | 0.56110(11) | 0.2000 | 0.825(1) | 15.61(56) | 0.0003(12) |

TABLE IX. Simulation parameters and results at $L/a = 8$.

| $\beta$ | $\kappa$ | Trajectories | Plaquette | $\delta\tau$ | Acceptance | $g^2_{\mathrm{SF}}$ | $M$ |
|---|---|---|---|---|---|---|---|
| 12.000 | 0.1283860 | 19,500 | 0.938309(12) | 0.1000 | 0.845(1) | 0.36679(56) | −0.00014(5) |
| 8.000 | 0.1298820 | 21,500 | 0.907231(14) | 0.0900 | 0.909(2) | 0.5763(10) | −0.00019(7) |
| 6.000 | 0.1314830 | 12,700 | 0.875942(18) | 0.0831 | 0.924(2) | 0.8137(26) | 0.00009(6) |
| 5.000 | 0.1328570 | 15,700 | 0.850755(16) | 0.0990 | 0.911(2) | 1.0250(83) | 0.00021(19) |
| 4.000 | 0.1351130 | 15,500 | 0.812644(20) | 0.1100 | 0.900(2) | 1.3886(93) | −0.00003(10) |
| 3.000 | 0.1394120 | 29,500 | 0.748734(28) | 0.1100 | 0.908(2) | 2.154(11) | −0.00002(18) |
| 2.500 | 0.1434820 | 52,100 | 0.697398(26) | 0.1430 | 0.843(2) | 3.000(18) | 0.00015(23) |
| 2.300 | 0.1458750 | 69,500 | 0.670656(21) | 0.1430 | 0.843(1) | 3.580(22) | 0.00026(20) |
| 2.200 | 0.1473293 | 69,500 | 0.655564(21) | 0.1430 | 0.840(1) | 4.020(31) | 0.00013(23) |
| 2.100 | 0.1489980 | 69,500 | 0.639127(23) | 0.1430 | 0.841(2) | 4.509(50) | 0.00028(29) |
| 2.000 | 0.1510138 | 208,900 | 0.621310(19) | 0.0495 | 0.834(1) | 5.452(42) | 0.00022(23) |
| 1.900 | 0.1533120 | 239,000 | 0.601863(21) | 0.1440 | 0.833(1) | 6.934(86) | 0.00008(32) |
| 1.825 | 0.1553190 | 268,900 | 0.586146(27) | 0.1430 | 0.834(1) | 9.46(15) | −0.00021(35) |
| 1.780 | 0.1566700 | 67,300 | 0.576453(74) | 0.1429 | 0.834(2) | 11.73(46) | −0.00333(90) |

TABLE X. Simulation parameters and results at $L/a = 12$.

| $\beta$ | $\kappa$ | Trajectories | Plaquette | $\delta\tau$ | Acceptance | $g^2_{\mathrm{SF}}$ | $M$ |
|---|---|---|---|---|---|---|---|
| 24.0000 | 0.1266100 | 57,900 | 0.969073(1) | 0.0667 | 0.764(2) | 0.17495(23) | 0.00004(1) |
| 12.0000 | 0.1280100 | 221,900 | 0.937972(1) | 0.0833 | 0.776(1) | 0.36828(27) | −0.00011(1) |
| 8.0000 | 0.1295000 | 173,900 | 0.906670(2) | 0.0909 | 0.792(1) | 0.58292(68) | 0.00005(1) |
| 7.0000 | 0.1301700 | 16,100 | 0.893197(5) | 0.0909 | 0.804(3) | 0.6801(27) | 0.00011(6) |
| 6.0000 | 0.1311000 | 46,500 | 0.875162(3) | 0.0909 | 0.833(3) | 0.8229(28) | 0.00016(4) |
| 5.0000 | 0.1324800 | 60,000 | 0.849816(4) | 0.1000 | 0.795(2) | 1.0328(35) | −0.00007(4) |
| 4.0000 | 0.1347120 | 62,500 | 0.811576(6) | 0.0900 | 0.835(4) | 1.4093(66) | 0.00028(6) |
| 3.5000 | 0.1364500 | 30,300 | 0.784117(10) | 0.1000 | 0.824(1) | 1.7137(76) | 0.00017(9) |
| 3.0000 | 0.1389850 | 33,500 | 0.747407(13) | 0.1111 | 0.779(3) | 2.205(20) | 0.00003(13) |
| 2.5000 | 0.1430440 | 94,500 | 0.695954(8) | 0.1000 | 0.842(3) | 3.128(31) | −0.00009(12) |
| 2.3000 | 0.1454255 | 72,100 | 0.669255(10) | 0.0909 | 0.855(1) | 3.776(40) | −0.00012(13) |
| 2.2000 | 0.1468380 | 109,400 | 0.654143(11) | 0.0900 | 0.829(5) | 4.28(49) | 0.00042(17) |
| 2.1000 | 0.1485305 | 121,200 | 0.637808(10) | 0.0881 | 0.838(5) | 4.96(82) | 0.00004(17) |
| 2.0000 | 0.1504620 | 60,000 | 0.619979(13) | 0.1111 | 0.768(2) | 5.97(19) | −0.00015(27) |
| 1.9500 | 0.1515450 | 310,600 | 0.610434(7) | 0.1111 | 0.821(3) | 7.06(11) | 0.00065(14) |
| 1.9000 | 0.1527400 | 272,900 | 0.600522(10) | 0.1111 | 0.802(2) | 8.20(16) | 0.00029(19) |
| 1.8500 | 0.1540370 | 409,600 | 0.590204(11) | 0.1111 | 0.828(2) | 10.92(24) | −0.00050(20) |
| 1.8000 | 0.1554310 | 199,500 | 0.579236(23) | 0.1111 | 0.758(1) | 17.37(96) | 0.00031(31) |
| 1.7500 | 0.1569430 | 442,000 | 0.567346(28) | 0.1111 | 0.744(4) | 59.5(5.6) | 0.00108(29) |

TABLE XI. Simulation parameters and results at $L/a = 16$.

| $\beta$ | $\kappa$ | Trajectories | Plaquette | $\delta\tau$ | Acceptance | $g^2_{\mathrm{SF}}$ | $M$ |
|---|---|---|---|---|---|---|---|
| 12.0 | 0.1278810 | 17,500 | 0.937768(4) | 0.0476 | 0.864(2) | 0.36802(68) | −0.00015(2) |
| 8.00 | 0.1293670 | 35,900 | 0.906361(1) | 0.0432 | 0.868(8) | 0.5844(18) | 0.00014(2) |
| 6.00 | 0.1309810 | 38,500 | 0.874761(2) | 0.0432 | 0.891(7) | 0.8269(34) | −0.00010(2) |
| 5.00 | 0.1323520 | 50,300 | 0.849347(2) | 0.0129 | 0.871(6) | 1.0566(52) | −0.00003(3) |
| 4.00 | 0.1345736 | 51,950 | 0.811008(3) | 0.0556 | 0.877(2) | 1.411(11) | 0.00033(4) |
| 3.00 | 0.1388563 | 32,300 | 0.746734(8) | 0.0171 | 0.883(4) | 2.217(33) | 0.00010(6) |
| 2.50 | 0.1428970 | 60,950 | 0.695290(6) | 0.0175 | 0.906(2) | 3.240(41) | 0.00023(10) |
| 2.30 | 0.1452748 | 64,700 | 0.668662(4) | 0.0623 | 0.873(1) | 3.924(71) | 0.00027(10) |
| 2.20 | 0.1467180 | 159,000 | 0.653642(4) | 0.0586 | 0.883(2) | 4.493(66) | 0.00045(7) |
| 2.10 | 0.1483940 | 150,700 | 0.637384(5) | 0.0664 | 0.854(1) | 5.128(86) | −0.00004(9) |
| 2.00 | 0.1503060 | 204,200 | 0.619621(4) | 0.0179 | 0.852(2) | 6.56(16) | 0.00051(11) |
| 1.90 | 0.1525678 | 210,100 | 0.600368(6) | 0.0229 | 0.826(1) | 9.66(30) | 0.00010(16) |
| 1.87 | 0.1533100 | 160,300 | 0.594175(10) | 0.0708 | 0.825(1) | 11.39(56) | 0.00029(22) |

TABLE XII. Simulation parameters and results at $L/a = 18$.

| $\beta$ | $\kappa$ | Trajectories | Plaquette | $\delta\tau$ | Acceptance | $g^2_{\mathrm{SF}}$ | $M$ |
|---|---|---|---|---|---|---|---|
| 8.00 | 0.1293410 | 32,500 | 0.906259(2) | 0.0526 | 0.852(2) | 0.5842(31) | −0.00015(2) |
| 6.00 | 0.1309400 | 20,450 | 0.874629(2) | 0.0714 | 0.752(4) | 0.8300(81) | 0.00014(4) |
| 5.00 | 0.1323100 | 20,000 | 0.849187(3) | 0.0714 | 0.765(4) | 1.046(11) | 0.00015(3) |
| 4.00 | 0.1345380 | 20,000 | 0.810827(4) | 0.0714 | 0.790(4) | 1.429(23) | 0.00031(5) |
| 3.00 | 0.1388350 | 60,150 | 0.746527(4) | 0.0769 | 0.803(5) | 2.301(25) | −0.00004(6) |
| 2.50 | 0.1429000 | 32,050 | 0.695148(6) | 0.0714 | 0.797(2) | 3.302(85) | −0.00082(13) |
| 2.30 | 0.1452385 | 55,700 | 0.668468(4) | 0.0625 | 0.842(2) | 4.10(12) | 0.00049(10) |
| 2.20 | 0.1466920 | 56,000 | 0.653523(5) | 0.0187 | 0.860(2) | 4.503(87) | 0.00018(11) |
| 2.10 | 0.1483490 | 74,500 | 0.637235(5) | 0.0582 | 0.857(1) | 5.44(14) | 0.00025(12) |
| 2.00 | 0.1502770 | 142,700 | 0.619592(5) | 0.1000 | 0.834(4) | 6.41(13) | 0.00002(11) |
| 1.95 | 0.1513521 | 234,200 | 0.610169(4) | 0.0625 | 0.830(1) | 8.15(27) | 0.00035(12) |
| 1.90 | 0.1525395 | 283,950 | 0.600432(5) | 0.0580 | 0.854(1) | 9.50(28) | −0.00054(11) |

TABLE XIII. Simulation parameters and results at $L/a = 24$.

| $\beta$ | $\kappa$ | Trajectories | Plaquette | $\delta\tau$ | Acceptance | $g^2_{\mathrm{SF}}$ | $M$ |
|---|---|---|---|---|---|---|---|
| 12.0 | 0.1277800 | 13,120 | 0.937558(1) | 0.0321 | 0.855(7) | 0.3721(18) | 0.00014(1) |
| 8.00 | 0.1292790 | 28,820 | 0.906050(1) | 0.0370 | 0.873(3) | 0.5992(34) | 0.00012(5) |
| 6.00 | 0.1308900 | 33,740 | 0.874360(1) | 0.0105 | 0.876(9) | 0.8323(76) | −0.00010(2) |
| 5.00 | 0.1322605 | 51,880 | 0.848876(1) | 0.0369 | 0.863(4) | 1.0505(95) | 0.00003(2) |
| 4.00 | 0.1344920 | 49,020 | 0.810465(2) | 0.0455 | 0.853(3) | 1.467(19) | 0.00003(6) |
| 3.00 | 0.1387840 | 51,360 | 0.746133(2) | 0.0124 | 0.877(2) | 2.337(52) | −0.00018(5) |
| 2.30 | 0.1451880 | 52,000 | 0.668165(3) | 0.0453 | 0.850(2) | 4.18(13) | 0.00045(6) |
| 2.20 | 0.1466400 | 45,900 | 0.653255(3) | 0.0147 | 0.845(2) | 4.56(16) | 0.00008(9) |
| 2.10 | 0.1483010 | 70,350 | 0.637084(3) | 0.0453 | 0.845(1) | 5.50(17) | −0.00009(7) |
| 2.00 | 0.1502180 | 214,710 | 0.619522(2) | 0.0667 | 0.841(1) | 6.99(23) | 0.00014(6) |
| 1.95 | 0.1513130 | 200,290 | 0.610297(2) | 0.0450 | 0.841(1) | 8.82(40) | −0.00072(8) |
| 1.90 | 0.1524597 | 225,460 | 0.600510(3) | 0.0476 | 0.819(1) | 10.95(57) | 0.00007(9) |

[1] S. Weinberg, Phys. Rev. D **13**, 974 (1976); L. Susskind, Phys. Rev. D **20**, 2619 (1979).

[2] E. Eichten and K. D. Lane, Phys. Lett. **90B**, 125 (1980); S. Dimopoulos and L. Susskind, Nucl. Phys. **B155**, 237 (1979).

[3] For reviews on the technicolor model, see, for example, R. S. Chivukula, arXiv:hep-ph/0011264; C. T. Hill and E. H. Simmons, Phys. Rep. **381**, 235 (2003); **390**, 553 (E) (2004); F. Sannino, *Dynamical Stabilization of the Fermi Scale* (Springer, Berlin, Heidelberg, 2013).

[4] M. E. Peskin and T. Takeuchi, Phys. Rev. Lett. **65**, 964 (1990); Phys. Rev. D **46**, 381 (1992).

[5] See, for example, R. S. Chivukula and E. H. Simmons, Phys. Rev. D **82**, 033014 (2010).

[6] G. Aad *et al.* (ATLAS Collaboration), Phys. Lett. B **716**, 1 (2012); S. Chatrchyan *et al.* (CMS Collaboration), Phys. Lett. B **716**, 30 (2012).

[7] B. Holdom, Phys. Rev. D **24**, 1441 (1981); K. Yamawaki, M. Bando, and K. i. Matumoto, Phys. Rev. Lett. **56**, 1335 (1986); T. W. Appelquist, D. Karabali, and L. C. R. Wijewardhana, Phys. Rev. Lett. **57**, 957 (1986); T. Akiba and T. Yanagida, Phys. Lett. **169B**, 432 (1986); M. Bando, T. Morozumi, H. So, and K. Yamawaki, Phys. Rev. Lett. **59**, 389 (1987).

[8] T. Appelquist, G. T. Fleming, and E. T. Neil, Phys. Rev. Lett. **100**, 171607 (2008).

[9] T. Appelquist, G. T. Fleming, and E. T. Neil, Phys. Rev. D **79**, 076010 (2009).

[10] T. Appelquist *et al.*, Phys. Rev. Lett. **106**, 231601 (2011).

[11] Z. Fodor, K. Holland, J. Kuti, D. Nogradi, and C. Schroeder, Phys. Lett. B **681**, 353 (2009); J. High Energy Phys. 11 (2009) 103.

[12] A. Deuzeman, M. P. Lombardo, and E. Pallante, Phys. Lett. B **670**, 41 (2008); Phys. Rev. D **82**, 074503 (2010).

[13] K. Miura, M. P. Lombardo, and E. Pallante, Phys. Lett. B **710**, 676 (2012).

[14] K. Miura and M. P. Lombardo, Nucl. Phys. **B871**, 52 (2013).

[15] Y. Shamir, B. Svetitsky, and T. DeGrand, Phys. Rev. D **78**, 031502 (2008); T. DeGrand, Y. Shamir, and B. Svetitsky, Phys. Rev. D **79**, 034501 (2009); **82**, 054503 (2010); **88**, 054505 (2013).

[16] T. DeGrand, Phys. Rev. D **80**, 114507 (2009); arXiv:1006.3777.

[17] X. Y. Jin and R. D. Mawhinney, Proc. Sci., LAT2009 (2009) 049.

[18] T. DeGrand and A. Hasenfratz, Phys. Rev. D **80**, 034506 (2009).

[19] A. Hasenfratz, Phys. Rev. D **80**, 034505 (2009).

[20] A. Hasenfratz, Phys. Rev. D **82**, 014506 (2010); Phys. Rev. Lett. **108**, 061601 (2012).

[21] A. Cheng, A. Hasenfratz, G. Petropoulos, and D. Schaich, J. High Energy Phys. 07 (2013) 061; arXiv:1303.7129.

[22] H. Ohki, T. Aoyama, E. Itou, M. Kurachi, C.-J. D. Lin, H. Matsufuru, T. Onogi, and E. Shintani *et al.*, Proc. Sci., LATTICE2010 (2010) 066.

[23] C.-J. D. Lin, K. Ogawa, H. Ohki, and E. Shintani, J. High Energy Phys. 08 (2012) 096.

[24] E. Itou, Prog. Theor. Exp. Phys. **2013**, 83B01 (2013); arXiv:1307.6645.

[25] A. J. Hietanen, J. Rantaharju, K. Rummukainen, and K. Tuominen, J. High Energy Phys. 05 (2009) 025.

[26] A. J. Hietanen, K. Rummukainen, and K. Tuominen, Phys. Rev. D **80**, 094504 (2009).

[27] L. Del Debbio, B. Lucini, A. Patella, C. Pica, and A. Rago, Phys. Rev. D **80**, 074507 (2009); **82**, 014509 (2010); **82**, 014510 (2010).

[28] F. Bursa, L. Del Debbio, L. Keegan, C. Pica, and T. Pickup, Phys. Rev. D **81**, 014505 (2010).

[29] K. i. Nagai, G. Carrillo-Ruiz, G. Koleva, and R. Lewis, Phys. Rev. D **80**, 074508 (2009).

[30] J. B. Kogut and D. K. Sinclair, Phys. Rev. D **81**, 114507 (2010).

[31] Y. Aoki, T. Aoyama, M. Kurachi, T. Maskawa, K.-i. Nagai, H. Ohki, A. Shibata, and K. Yamawaki, T. Yamazaki, Phys. Rev. D **85**, 074502 (2012); **86**, 054506 (2012).

[32] K.-I. Ishikawa, Y. Iwasaki, Y. Nakayama, and T. Yoshie, Phys. Rev. D **87**, 071503 (2013); arXiv:1304.4345.

[33] S. Ejiri and N. Yamada, Phys. Rev. Lett. **110**, 172001 (2013).

[34] F. Bursa, L. Del Debbio, L. Keegan, C. Pica, and T. Pickup, Phys. Lett. B **696**, 374 (2011).

[35] T. Karavirta, J. Rantaharju, K. Rummukainen, and K. Tuominen, J. High Energy Phys. 05 (2012) 003.

[36] G. Voronov, Proc. Sci., LATTICE2012 (2012) 039.

[37] M. Hayakawa, K.-I. Ishikawa, Y. Osaki, S. Takeda, S. Uno, and N. Yamada, Phys. Rev. D **83**, 074509 (2011).

[38] M. Hayakawa, K.-I. Ishikawa, Y. Osaki, S. Takeda, and N. Yamada, Proc. Sci., LATTICE2012 (2012) 040.

[39] M. Hayakawa, K.-I. Ishikawa, S. Takeda, M. Tomii, and N. Yamada, arXiv:1307.6696 [Phys. Rev. D (to be published)].

[40] M. Fukugita, S. Ohta, and A. Ukawa, Phys. Rev. Lett. **60**, 178 (1988).

[41] F. R. Brown, H. Chen, N. H. Christ, Z. Dong, R. D. Mawhinney, W. Schaffer, and A. Vaccarino, Phys. Rev. D **46**, 5655 (1992).

[42] Y. Iwasaki, K. Kanaya, S. Kaya, S. Sakai, and T. Yoshie, Phys. Rev. D **69**, 014507 (2004).

[43] M. Luscher, R. Narayanan, P. Weisz, and U. Wolff, Nucl. Phys. **B384**, 168 (1992); S. Sint, Nucl. Phys. **B421**, 135 (1994); M. Luscher, R. Sommer, P. Weisz, and U. Wolff, Nucl. Phys. **B413**, 481 (1994); M. Luscher, S. Sint, R. Sommer, and P. Weisz, Nucl. Phys. **B478**, 365 (1996).

[44] S. Sint and P. Weisz (ALPHA Collaboration), Nucl. Phys. **B545**, 529 (1999); S. Capitani, M. Lüscher, R. Sommer, and H. Wittig (ALPHA Collaboration), Nucl. Phys. **B544**, 669 (1999); M. Della Morte, R. Hoffmann, F. Knechtli, J. Rolf, R. Sommer, I. Wetzorke, and U. Wolff (ALPHA Collaboration), Nucl. Phys. **B729**, 117 (2005).

[45] For a more comprehensive discussion on the perturbative results, see, for example, T. A. Ryttov and R. Shrock, Phys. Rev. D **83**, 056011 (2011).

[46] C. Pica and F. Sannino, Phys. Rev. D **83**, 035013 (2011).

[47] T. A. Ryttov, arXiv:1309.3867.

[48] T. van Ritbergen, J. A. M. Vermaseren, and S. A. Larin, Phys. Lett. B **400**, 379 (1997).

[49] J. A. M. Vermaseren, S. A. Larin, and T. van Ritbergen, Phys. Lett. B **405**, 327 (1997).

[50] M. Luscher, R. Sommer, U. Wolff, and P. Weisz, Nucl. Phys. **B389**, 247 (1993).

[51] M. Hayakawa, K.-I. Ishikawa, Y. Osaki, S. Takeda, S. Uno, and N. Yamada, Proc. Sci., LATTICE2010 (2010) 325.

[52] S. Sint and P. Vilaseca, Proc. Sci., LATTICE2011 (2011) 091; LATTICE2012 (2012) 031.

[53] A. Bode, P. Weisz, and U. Wolff (ALPHA Collaboration), Nucl. Phys. **B576**, 517 (2000); A. Bode, P. Weisz, and U. Wolff (ALPHA Collaboration), Nucl. Phys. **B600**, 453 (E) (2001); A. Bode, P. Weisz, and U. Wolff (ALPHA Collaboration), Nucl. Phys. **B608**, 481(E) (2001).

[54] S. Aoki *et al.* (PACS-CS Collaboration), J. High Energy Phys. 08 (2010) 101.

[55] E. Shintani, S. Aoki, H. Fukaya, S. Hashimoto, T. Kaneko, H. Matsufuru, T. Onogi, and N. Yamada (JLQCD Collaboration), Phys. Rev. Lett. **101**, 242001 (2008).